ABSTRACT

Title of Document: IMPROVING PHOTOVOLTAICS WITH HIGH LUMINESCENCE EFFICIENCY QUANTUM DOT LAYERS

James Chen, DJ Gagner, Kevin Griffiths, Emily Hitz, Akira Horiguchi, Ryan Joyce, Byung Yub Kim, Michael Lee, Seongwoo Lee, Alex Raul, DoRonne Shyu, Zachary Siegel, Steven Silberholz, Douglas Tran

Directed by: Dr. Jeremy Munday, Ph.D
Department of Electrical and Computer Engineering, Institute for Research in Electronics and Applied Physics and Chemical Physics Graduate Program

A solar cell relies on its ability to turn photons into current. Because short wavelength photons are typically absorbed near the top surface of a cell, the generated charge carriers recombine before being collected. But when a layer of quantum dots (nanoscale semiconductor particles) is placed on top of the cell, it absorbs short wavelength photons and emits them into the cell at longer wavelengths, which enables more efficient carrier collection. However, the resulting power conversion efficiency of the system depends critically on the quantum dot luminescence efficiency – the nature of this relationship was previously unknown. Our calculations suggest that a quantum dot layer must have high luminescence efficiency (at least 80%) to improve the current output of existing photovoltaic (PV) cells; otherwise, it may worsen the cell's efficiency. Our quantum dot layer (using quantum dots with over 85% quantum yield) slightly reduced the efficiency of our PV cells. We observed a decrease in short circuit current of a commercial-grade cell from 0.1977 A to 0.1826 A, a 7.6% drop, suggesting that improved optical coupling from the quantum dot emission into the solar cell is needed. With better optical coupling, we predict current enhancements between ~6% and ~8% for a solar cell that already has an antireflection coating. Such improvements could have important commercial impacts if the coating could be deployed in a scalable fashion.

Citation Style: CSE

IMPROVING PHOTOVOLTAICS WITH HIGH LUMINESCENCE EFFICIENCY QUANTUM DOT LAYERS

Team QUANTUM SEA
(Quantum Dot Usage as a New Technique to Unleash Maximum Solar Energy Absorption)

James Chen, DJ Gagner, Kevin Griffiths, Emily Hitz, Akira Horiguchi, Ryan Joyce, Byung Yub Kim, Michael Lee, Seongwoo Lee, Alex Raul, DoRonne Shyu, Zachary Siegel, Steven Silberholz, Douglas Tran

Mentor: Jeremy Munday

Thesis submitted in partial fulfillment of the requirements of the
Gemstone Program, University of Maryland, 2015

Advisory Committee:
Dr. Jeremy Munday, University of Maryland, Mentor
Dr. Liangbing Hu, University of Maryland
Dr. Raymond Adomaitis, University of Maryland
Dr. Mario Dagenais, University of Maryland

Acknowledgements

We thank our mentor Professor Jeremy Munday for giving us the freedom to pursue our ambitions while advising us through our problems and goals, which granted us the truest research experience an undergraduate team could have. We also thank graduate students Joe Murray for helping us build our own problem solving skills, Dongheon Ha for his lab expertise and for the extensive time he took to verify our data collection procedure, Yunlu Xu for his help implementing the Drude-Lorentz model, and Professor Min Ouyang for his quantum dot fabrication expertise. We thank the FabLab, in particular John Abrahams, John Hummel, and Tom Loughran, for providing crucial lab space, equipment, and expertise. We thank UMD's Office of Sustainability and ACC Fellows Program in Creativity and Innovation for funding our lab time and materials. We thank our defense panel members for taking the time to provide their expertise and feedback. Finally, we thank the Gemstone program, in particular Dr. Frank Coale, Dr. Kristen Skendall, Vickie Hill, and Alex Winter, for uniting 14 undergraduate students toward a shared goal.

Contents

CHAPTER 1 – INTRODUCTION

The modern era is marked by a great demand for energy, the largest part of which is satisfied by the combustion of non-renewable fossil fuels. If the energy demand of the United States, China, and India all continue increasing at their current rates, oil consumption will reach 180 million barrels of oil per day by 2050[1]. Such heavy oil consumption will release an overwhelming amount of heat-trapping greenhouse gases, resulting in "irreversible dry-season rainfall reductions … and inexorable sea level rise"[2, 3]. In addition, oil is a finite resource and the increasing demand for oil will eventually exceed maximum global production. The resulting increase in fuel cost could stagnate economic growth, and if no action is taken in response to this energy crisis, "the global economy could shrink by between 5% and 20% over the next two centuries"[4].

As the shortcomings of our current reliance on fossil fuel energy become more apparent, it is imperative that we look to alternative energy sources to meet our demand for power. However, wind, tidal, and hydroelectric power are too dependent on geographic location to be globally applicable. Relying on nuclear power only replaces one exhaustible fuel with another, while creating concerns over radioactive waste storage and security. Of all the known alternative sources of energy, solar power is best positioned to sustainably meet the world's future energy needs. About 1.37 kW/m^2 is incident on the earth from the sun[5-7]. Even after considering the energy lost from the solar flux traveling through the atmosphere, more energy is received on the "earth's surface in one and a half hours…than worldwide energy consumption in the year 2001 from all sources combined."[5,7].

However, a major factor inhibiting solar power usage is the cost of power ($/W). A typical single-junction **photovoltaic (PV)** solar cell operates at only about 13-18% efficiency[5],

whereas an ideal single-junction PV cell would have a maximum power conversion efficiency of about 33.5%[5]. This upper bound is known as the Shockley-Quiesser limit and depends only on the **bandgap** of the semiconductor and the particular distribution of wavelengths found in sunlight (Figure 1.1) [5,6,8].

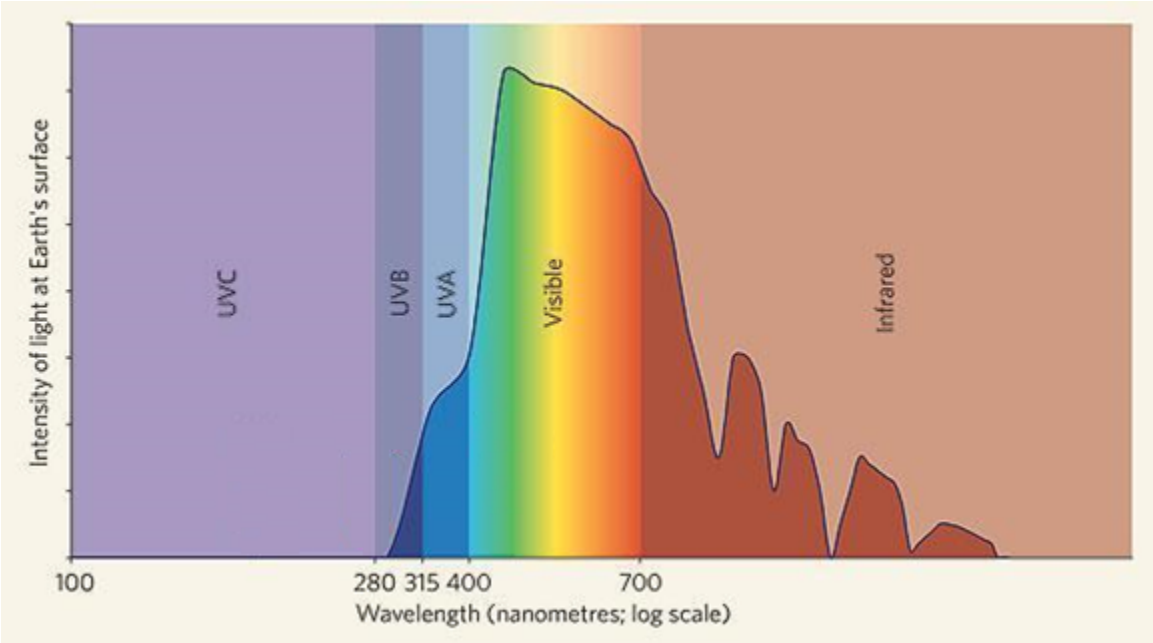

Figure 1.1. Distribution of solar radiation across the electromagnetic spectrum[9].

There are several obstacles inhibiting PV cell efficiency; for this project, we will focus on two. The first obstacle is photon loss due to light reflecting from the surface of the cell. An effective **anti-reflection coating (ARC)** reduces this reflection and thereby increases the cell's energy output[10]. This can be done by choosing a material with an appropriate **index of refraction** and layer thickness to minimize surface reflection[10]. A second obstacle is the loss of carriers generated by high-energy photons near the front surface. While light is absorbed throughout the cell, high-energy photons tend to be absorbed near the front of the cell. However, electron-hole pairs generated near the surface are more likely to recombine and hence are less efficiently collected.

Semiconductor nanoparticles called **quantum dots (QDs)** offer a promising new way to solve these problems. A key benefit of using QDs is that they **downshift** (also called **fluorescence**), a process that takes higher energy photons and converts them into lower-energy photons. Much like anti-reflection, downshifting can occur in the additional layer that is applied to the surface of a PV cell, so it can convert photons that the cell cannot effectively utilize into ones that it can readily absorb deeper within the semiconductor (Figure 1.2). In one study, cadmium sulfide (CdS) QDs were coated onto gallium arsenide (GaAs) PV cells, which increased the cells' efficiency by as much as 18.9%[11].

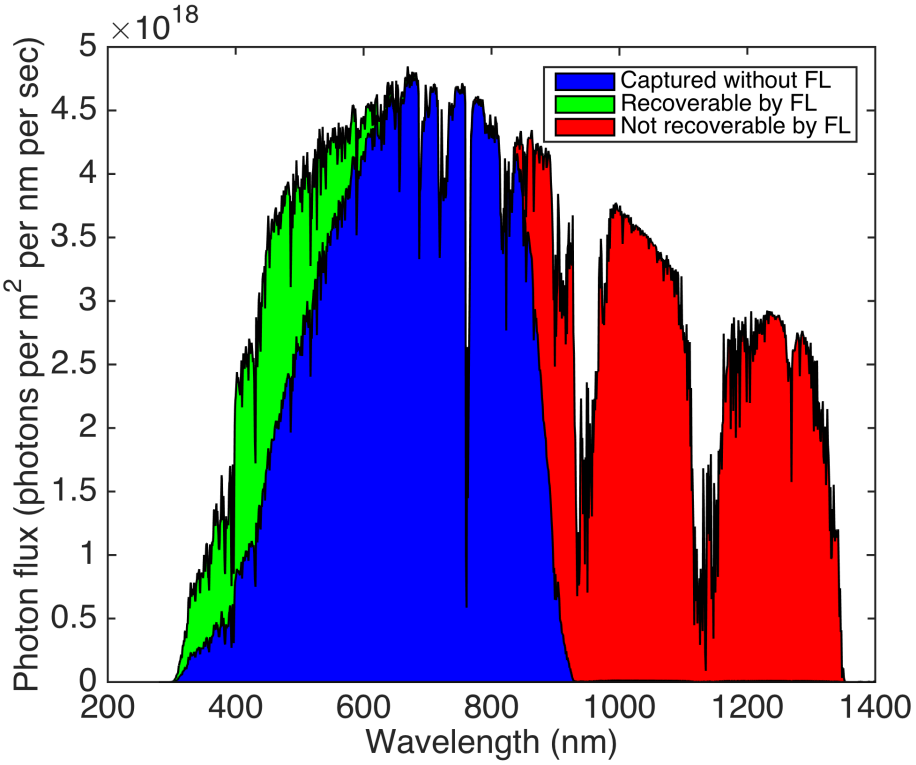

Figure 1.2. AM 1.5G solar spectrum[12]. A cell can convert some photons into current without a downshifting layer (blue, middle) but cannot use the remaining photons. With a downshifter, a cell can convert additional photons (green, left) into current. The remaining photons (red, right) are not recoverable even with a downshifting layer.

Moreover, QDs possess the unique property that their size influences their electronic structure and absorption and emission properties. Instinctively, a material's properties, including

its density, emission color, and melting point, are dependent on its material composition rather than size or shape, but this intuition fails at the quantum scale. Varying the size of quantum dots without changing the material enables us to manipulate the bandgaps of QDs and thus the photon frequencies at which they absorb and emit (Figure 1.3)[13]. The unique versatility of QDs greatly simplifies the complicated and expensive process of formulating composite materials with the desired bandgap. After determining the required bandgap, the only parameter that needs to be selected is the size of the QDs[13].

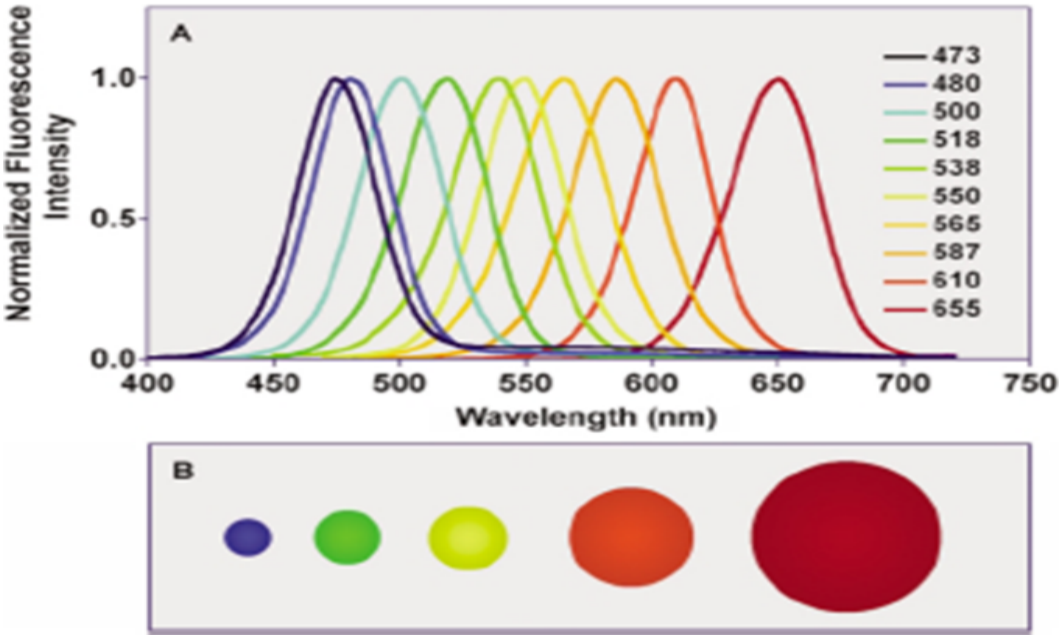

Figure 1.3. Schematic comparison of QD size to its emission peaks through color[13]. Larger QDs have a peak emission at longer wavelengths, while smaller QDs peak at shorter wavelengths.

Layers embedded with QDs also display impressive anti-reflection properties. Recently, several research groups have implemented QDs in anti-reflection films, successfully lowering reflection percentages of cells from approximately 40% to 5%, an improvement comparable to that of applying conventional anti-reflection coatings[15]. This demonstrates the viability of QDs as a next generation alternative to current anti-reflection films.

Our research originally sought to answer the following question: How can a dual-purpose

quantum dot-based fluorescent, anti-reflection coating be incorporated into bare PV cells to improve solar cell efficiency, and by how much can the efficiency improve? We hypothesized that by adding a dual-purpose QD layer to a PV cell, we could convert many high-energy photons into lower-energy photons the cell can more easily turn into current and provide anti-reflection for photons throughout the visible region. We ultimately modified our experimental design to test whether consumer-grade solar cells could benefit from having a quantum dot layer applied to them. The PV cells we used were manufactured with an anti-reflection layer. We examined whether a second layer with fluorescent QDs would result in an efficiency increase. Specifically, when a quantum dot-based fluorescent coating is applied to a commercial PV cell that already has a traditional anti-reflection layer, how does the QD concentration affect the cell's efficiency? We hypothesized that a high density of high quality QDs is needed to observe a significant increase in efficiency of the consumer PV cells.

CHAPTER 2 - LITERATURE REVIEW

The past forty years have seen an extensive exploration of PV technology and the use of anti-reflection layers in improving its effectiveness[15-19]. With such advances in technology, scientists have been able to address many of the factors that can degrade the efficiency of the solar energy harvesting process. Using fluorescence from quantum dots for PV applications, however, has only taken root in the last few years. In this section, we provide background information on light and how solar cells function. We present fabrication techniques, previous work by others, our testing protocol, and apparatuses needed to study QD fluorescent anti-reflection films for solar cells. Finally, we discuss our intended contribution to the field.

2.1 Theory of Solar Power Generation

To establish a reliable energy supply for the future, scientists must find a way to harness solar power effectively and economically. An early connection between light and electricity was established in 1839 when Edmund Becquerel demonstrated that certain materials generate an electrical voltage when exposed to light[20]. The connection was further developed in 1876 when William Grylls Adams and Richard Evans Day showed that light by itself could generate an electric current. To fully harness solar energy, scientists had to develop an understanding of the principles of light and how to convert it into usable electricity.

James Clerk Maxwell provided a critical understanding of light in his 1865 paper[21] and showed mathematically that light moves as an electromagnetic wave (Figure 2.1), a description that successfully explains many optical phenomena. When light hits a metal surface, electrons are emitted, a process known as the photoelectric effect. Several experiments showing electron ejection from a metal under illumination in the late 1800s led Albert Einstein to postulate that

light is not made of a continuous stream of material, but rather it is made of discrete particles of energy called photons[21]. Robert Millikan verified Einstein's predictions by showing that the emission of electrons from a metal is independent of the incident light intensity and by describing the functional form of the frequency dependence of this effect[23]. Einstein's particle-description of light explains these observations; an electron can escape the metal only if it absorbs a photon with enough energy. The electron's escape does not depend on the intensity of the light, but rather on the incident photon's wavelength. The energy of a photon is given by $E_{ph}=\frac{hc}{\lambda_{ph}}$, where h is Planck's constant, c is the speed of light, and λ_{ph} is the wavelength of the photon. Photons with a short wavelength have high energy while photons with a long wavelength have low energy.

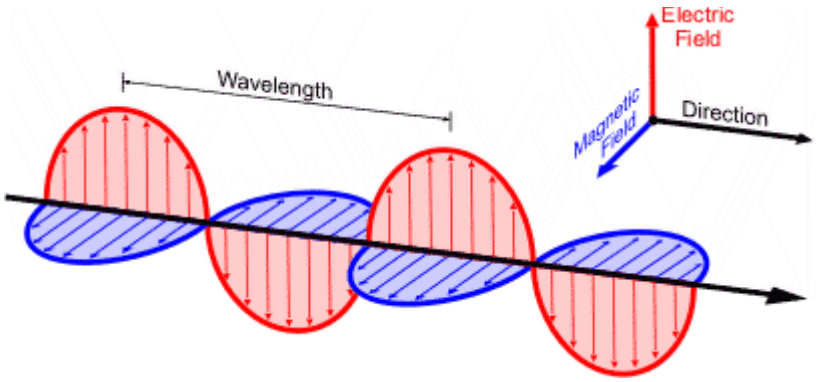

Figure 2.1. Depiction of light as the propagation of an oscillating electric field and magnetic field[24].

2.2 Solar Cells

Solar cells are semiconductor devices capable of absorbing light and converting the energy of the photons into usable electricity. When a photon with enough energy is absorbed within the cell, it excites an electron into the conduction band of the material. The conduction

band describes the energy state at which electrons can move freely under the influence of an electric field. The excited electron also leaves behind a 'hole,' which acts as a positive charge carrier. The electron-hole pair dissociates, and the individual entities (the electron and the hole) travel to opposite terminals, which create the current to power an external device (Figure 2.2).

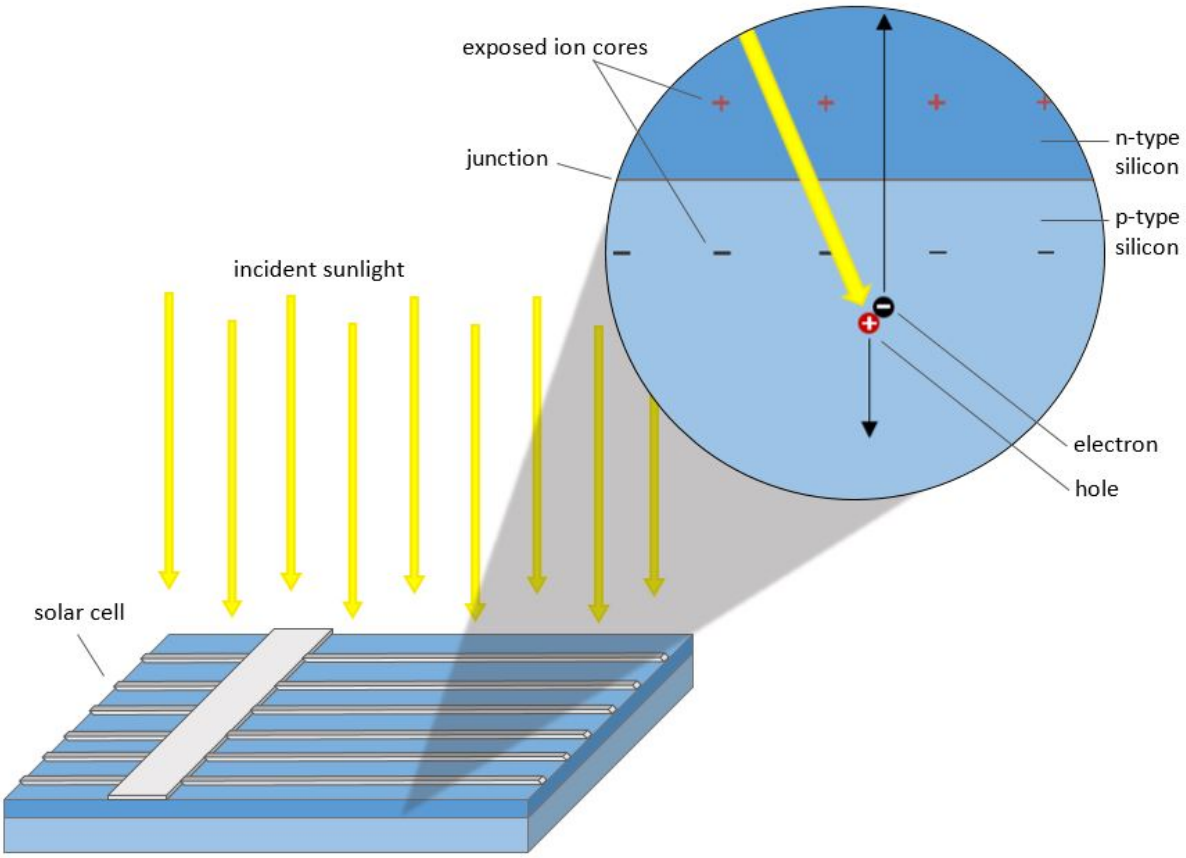

Figure 2.2. A photon is absorbed within the cell, which excites an electron-hole pair to create current.

Solar cells are manufactured into two types of silicon cells: monocrystalline cells and polycrystalline cells. Monocrystalline cells are composed of a single uniform crystalline lattice of silicon, while polycrystalline cells are composed of multiple crystalline lattices of silicon. The manufacturing of monocrystalline cells require a more careful and time consuming procedure which results in higher pricing, but these cells usually exhibit more uniform current generation and higher efficiency than their polycrystalline counterparts. Polycrystalline cells are

significantly cheaper compared to monocrystalline cells due to a simplified manufacturing method. Polycrystalline cells have grain boundaries, which are the division lines that exist between the multiple crystalline structures within the cell. These boundaries are considered obstructions within a possible uniform crystalline structure, which affects both the electrical and thermal properties of the polycrystalline cell.

We conducted experiments on polycrystalline cells and found inconsistent measurements, which we attributed to the inherent variation in size and arrangement of grains within a polycrystalline cell. To address this issue, we instead used monocrystalline cells for their uniform microstructure and observed more consistent data. In addition to producing more consistent data, we found monocrystalline cells easier to dice into smaller sample cells for our experiments. Hence, we exclusively used monocrystalline cells for the data presented in this thesis[20].

2.3 Quantum Dots

2.3.1 Anti-reflection

A critical method of maximizing solar cell efficiency is adding a film that reduces the amount of light reflected off of the surface of a solar cell[17]. These coatings are chosen by varying the thickness and the refractive index of the film. In our work, we hold the refractive index constant. We were also unable to control the thickness of our layer to the precision needed for optimizing anti-reflection. Instead, we focused on varying the concentration of QDs to maximize the cell's efficiency based on the emission of luminescent photons rather than the anti-reflection effects. However, we include a discussion of anti-reflection as it is an important consideration for photovoltaics in general.

Every material has a particular index of refraction. When light passes from one bulk

material to another, the amount of reflected light is greater when the difference between their indices of refraction is larger. Hence, to minimize the amount of light reflected when sunlight hits the surface of a PV cell, an anti-reflection layer should have an index of refraction between that of the surface and that of air[25].

As mentioned previously, light incident on a solar cell can be modeled as a wave. For an anti-reflection layer to be effective, the light that would normally be reflected should **destructively interfere** with itself (Figure 2.3). If this condition is achieved, less **incident light** is reflected. This allows a PV cell to capture more photons, thereby increasing the overall efficiency of the cell[10].

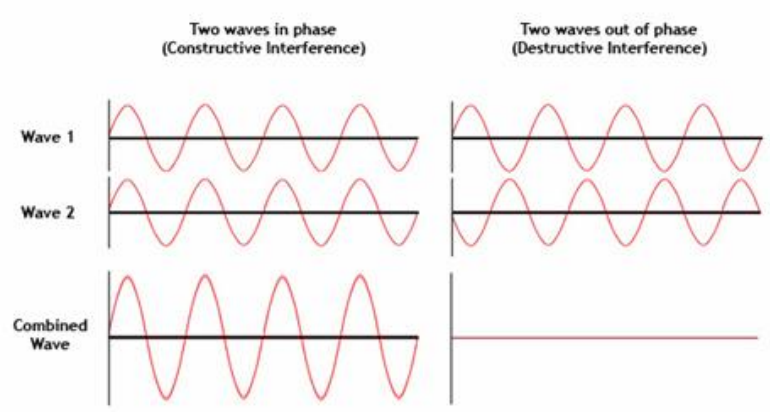

Figure 2.3. A graphical representation of constructive (left) and destructive (right) interference. For destructive interference the two light waves have peaks and troughs at opposite phases and lead to cancellation[25].

To minimize reflection from the top of a solar cell, a material with an index of refraction between that of air and that of the PV cell must be selected[25]. The choice of an appropriate thickness further minimizes the reflection of certain wavelengths of light through destructive interference. Typically this wavelength is chosen near the peak of the solar spectrum to maximize the absorption within the cell.

While a single material having an intermediate index of refraction can be used to

accomplish anti-reflection, other techniques can be used to reduce the loss of light incident on a PV cell. Of particular interest to this research is the consideration of composite QD layers for increased anti-reflection performance capabilities. Rather than using a single layer composed of one material, one can create a thin film containing fluorescent QDs that reduces reflection. One research team recently created a multifunctional film using silicon QDs and silicon dioxide (SiO_2), and observed significant improvement in absorption in the underlying silicon cell[15]. These multifunctional films are preferable because they can potentially reduce production costs and can address several problems at once, as Vikram Iyengar and his team demonstrated by streamlining the processes for **doping**, anti-reflection, and **surface passivation**[18]. This is an important step towards meeting cost reduction targets for manufacturing high efficiency PV cells.

Moreover, cells coated with QD films such as those created by embedded CdS QDs provide "a superior anti-reflective property" at visible wavelengths compared to cells without QDs[26]. Thus, QD composite layers have the potential to improve PV cell efficiency because they can yield increased performance as anti-reflection coatings in addition to their intrinsic luminescent properties, which are most relevant to our research. A QD-based front surface fluorescent layer was recently designed by Jung *et al.* and demonstrated a 13% improvement in power conversion efficiency when applied via spin coating to a silicon cell[27]. Again we note that the use of QD layers for anti-reflection is not within the scope of our experiments because we used commercial cells that already had anti-reflection coatings.

2.3.2 Fluorescence

Research in recent years suggests that QDs applied from a colloidal solution benefit both from easy tuning of electronic properties (such as bandgap) and low-cost fabrication[28]. Thus,

QDs could be a critical factor in making solar energy a viable source of renewable energy. Because QDs exhibit the property of fluorescence, they are of particular interest when considering possible technologies for improving photovoltaics. A material that has fluorescence capabilities absorbs high energy photons and re-emits them at a lower energy (Figure 2.4). By extending this idea to a fluorescent anti-reflection layer applied to an existing solar cell, scientists have been able to increase the overall solar energy absorption of a traditional cell with the addition of such a layer[27].

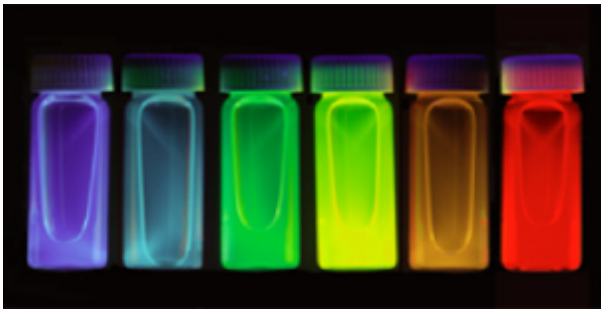

Figure 2.4. Vials containing colloidal solutions of CdSe quantum dots. The quantum dots in each vial fluoresce at a particular wavelength[29]. The predominant color of emitted light is altered by varying the size of the quantum dots.

The process of luminescence is common in a variety of materials, including dyes and QDs. Luminescent dyes have been used in optical concentrating systems, but are prone to degradation over the lifetime of the material. As an alternative, QDs have the advantage of large absorption bands, narrow spectral emission bands, and photochemical stability. In other words, QDs absorb a wider range of high-energy photons, emit a more precise range of low-energy photons, and ensure a longer product lifetime under continual photon bombardment[30]. This would allow for the QDs to continually absorb photons of higher energy and re-emit them at lower energy that is within the cell's capability to absorb efficiently (Figure 2.5).

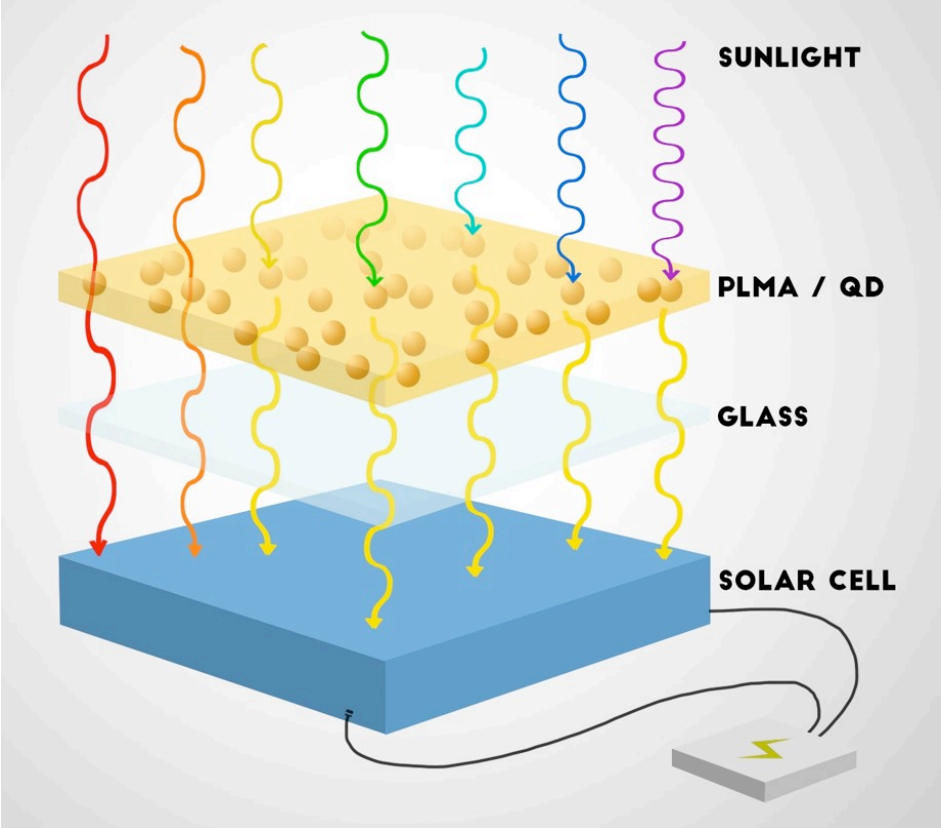

Figure 2.5. Schematic of QD-treated solar cell. The layer is illuminated with short and long wavelength photons in the solar spectrum. The quantum dots absorb this light, and re-emit it at longer wavelengths into the solar cell.

Cadmium sulfide (CdS) and cadmium selenide (CdSe) quantum dots are two promising QD materials for use in fluorescence. Spin-coating CdS QDs onto the surface of a gallium arsenide (GaAs) PV cell as a fluorescent and anti-reflection film was found to improve the efficiency of the cell by 2.7% over an optimal anti-reflection coating, and 18.9% over a bare GaAs cell without a coating[11]. These effects can greatly improve the **external quantum efficiency (EQE)** for high-energy (short-wavelength) photons and merits further study[31].

An alternative use of quantum dots for PV applications can be found in down-conversion, a process by which one high-energy photon is absorbed and two low-energy photons are emitted. A 2002 model by Trupke, Green, and Wurfel calculated that the theoretical maximum efficiency of 30.9% of a single-junction semiconductor PV cell (with a bandgap of 1.1 eV) could be

improved to as much as 38.6% with the addition of a front surface-mounted down-converter[8]. In the field of PV, where generational improvements in solar cells often involve increases of no more than 1% efficiency, this improvement was a startling revelation[31]. Scientists have explored the use of other materials, such as rare-earth metals, that can act as down-converters. Unfortunately, the efficiency of these materials has been low and ineffective[32,33]. Currently, there is not conclusive evidence that QDs can act as efficient down-converters to yield a significant improvement in a PV device.

2.3.3 Thin Films

Thin films for diluting concentrations of QDs are commonly created from one of two polymers: Polymethyl methacrylate (PMMA) or Polylauryl methacrylate (PLMA). Both polymers have been used as mediums for fluorescent layers in PV applications. However, researchers found that embedding quantum dots in PMMA caused fast luminescence quenching, while the QDs embedded within PLMA retained their quantum efficiency[34]. Hence, we chose PLMA as our thin film polymer.

2.4 Spin coating

Spin coating is a process commonly used in various industries to create a uniformly thin layer of film onto flat substrates. The layer's thickness can range from micrometers to nanometers. One can dictate its thickness with proper control of spin speed, time, etc. during the coating process.

There are four phases of spin coating, which can be broken down as deposition, spin-on, spin-off, and evaporation. The deposition phase involves depositing the solution onto the surface

of the substrate. The solution is typically applied so that a layer initially coats the entire surface of the sample with a large amount of the solution at the center of the substrate[35].

The spin-up phase rotationally accelerates the substrate to the desired spin speed. In this phase, a significant fraction of the solution is ejected from the surface of the substrate due to the rotational motion. As the substrate spins, the solution layer begins to gradually decrease in thickness until it can co-rotate with the substrate. This co-rotation evens out the layer thickness at the surface. At this point, the rotational acceleration is in complete balance with the viscous shear drag.

The spin-off phase or the stable fluid outflow phase is when the substrate has reached its final velocity where the thinning of the layer is dominated by the fluid viscous forces. The phase is characterized by a gradual, uniform thinning of the layer, which slows as the thickness of the layer is reduced. It is common to visually observe both optical interference and an accumulation at the corners of a rectangular substrate during this phase. The height and width of this aggregation is dependent on the surface tension and viscosity of the solution, as well as the rotation rate of the substrate. Because this phenomenon is restricted to the edges, leaving the bulk of the coated layer unaffected, we found the irregularities to be acceptable.

When the spin-off phase is complete, the procedure moves into the evaporation phase. In the evaporation phase, the layer begins to dry and the primary source of film thinning is due to the evaporation of the solvent. The substrate is spinning at a constant speed, and the rate of evaporation is determined primarily by the partial pressure in the solvent between the free surface of the liquid layer and the surrounding atmosphere. The process is complete after the solvent has completely evaporated from the substrate, leaving only a highly viscous layer.

There are quite a few advantages to spin coating. The first, and perhaps most important,

is the ease with which the thickness can be changed: by simply modifying the rotational speed of the substrate, the experimenter can change the layer thickness. In addition, spin coating produces a more uniform layer compared to other coating methods[35]. As the layers become thinner, the variability of its thickness reduces. When compared to other coating methods, spin coating proves to be a reasonable choice, given its cost-effectiveness for laboratory fabrication of small experimental batches and the simplicity of the technique.

The two main disadvantages of spin coating are its restriction on large area coverage and the amount of solution lost through the process. When considering coating a large substrate, the limitation that the spin coating technique introduces is the difficulty in maintaining a thin and functionally uniform layer. When examining the coating process in terms of solution, only 2-5% is actually used to form the layer, while the other 95-98% is lost in the rotation. This is a significant disadvantage when considering the efficiency of the procedure – such a loss can be costly and ineffective in large-scale coating; however, reclaiming waste solution can mitigate material loss.

2.5 Summary of Literature Review

While QDs have many diverse applications in the field of photovoltaics, Team QUANTUM SEA has focused on using them in a thin film to improve the EQE of a PV cell under sunlight. The QDs in the film convert high-energy photons into lower energy photons that the solar cell can use more efficiently, increasing the overall current (and thus, power) generated[26]. QUANTUM SEA sought to increase solar cell efficiency using this concept. Any such progress in this direction will help meet rising energy demands and replace nonrenewable energy sources.

CHAPTER 3 – METHODOLOGY

3.1 Introduction

To obtain repeatable and accurate results, we developed a systematic experimental procedure to test our hypothesis. To reduce user error, we grouped into teams that specialized in parts of the overall procedure. Details on each step of this procedure can be found in the subsequent subsections.

To demonstrate an increase in efficiency, we had to select the appropriate materials. Using the MATLAB scripts we wrote to facilitate our calculations, we predicted the performance of the QDs purchased for application onto our purchased monocrystalline silicon solar cells. We used monocrystalline silicon solar cells to reduce error due to variation in lower quality cells.

The first step in the laboratory was dicing the solar cells to an appropriate size for the testing equipment. Next, to deposit the QDs onto the solar cell, we dispersed them in a polymer solution that we could spin coat onto the cell. Once the solution had dried, we analyzed and characterized the layer.

We measured the EQE and current-voltage (IV) characteristic of cell samples before and after the application of the layer to measure the effect of cell coating.

3.2 Dicing Solar Cells

Due to size limitations of the spin coater's vacuum chuck, the existing 5"x5" solar cells were diced to dimensions of 1"x1" (Figure 3.1). Dicing the cells also helped to prevent damage during handling and reduced the overall cost of experimentation by conserving material. To cut wafer-sized cells to precise smaller dimensions, we used the Model 1006A MicroAutomation Industries Wafer Dicing Saw. The saw cut uniformly sized cells from our monocrystalline silicon

solar cells. The diced cells, which contained sections of the busbars of the original cell, were then used for experimentation.

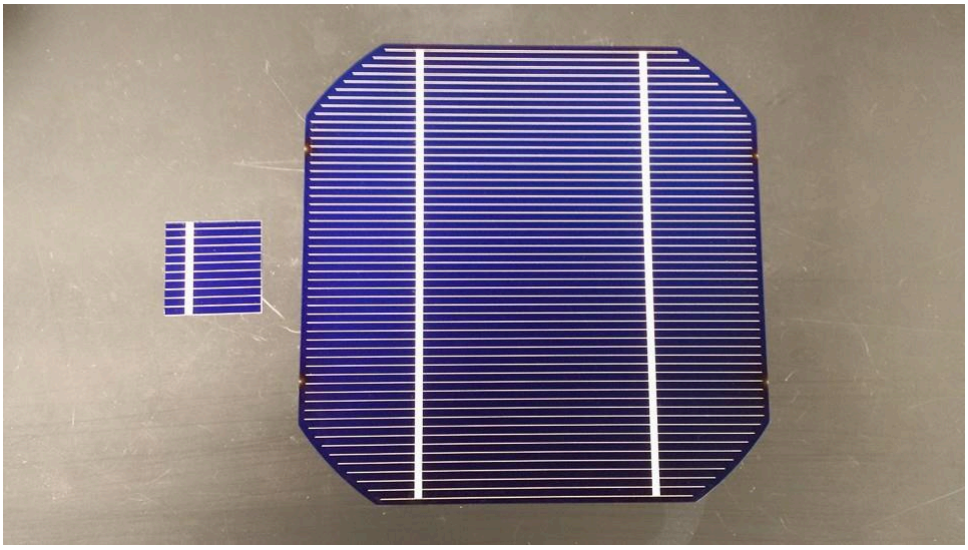

Figure 3.1. Comparison between a diced cell (left) and a full solar cell (right).

3.3 Cell Coating and Layer Fabrication

3.3.1 Formulating the Cell Coating

To ensure consistent measurement of the quantity of QDs used for each sample, we chose to work with colloidal quantum dots already in solution. Using quantum dots in solution also simplified mixing the solution with PLMA. We purchased two vials of CdSe/ZnS core-shell QDs from NN-Labs with emission peaks at 520 and 620 nm with a concentration of 20 mg quantum dot to 1 mL toluene. Each vial contained 0.5 mL of toluene and 10 mg of quantum dots. Our target concentration for our solution was 20 mg quantum dots to 1 mL of PLMA. We chose to use core-shell QDs for superior chemical stability over the single-material variety.

As each vial already contained 10 mg quantum dots and 0.5 mL of toluene, we wanted to add 0.5 mL of PLMA to each vial. Because the PLMA solution was 28.8% PLMA and 71.2% toluene, 1.736 mL of PLMA solution was added to each vial so that the ratio between quantum

dots to PLMA was 20 mg quantum dot to 1 mL of PLMA. After the correct amount of PLMA was added, each vial was stirred for several minutes in order to ensure a homogeneous mixture.

3.3.2 Spin coating

Our sample set was composed of two groups: the first group consisted of monocrystalline silicon solar cells onto which we directly applied the quantum dot and PLMA mixture, and the second group consisted of monocrystalline silicon solar cells that used a glass layer as the medium onto which the quantum dot and PLMA mixture was applied. The samples using the coated glass cover slides were included as part of the experimental set after initial experimentation with the direct-coated cells yielded significant cell-to-cell variation. The glass slides allowed for greater control in the fabrication, characterization, and testing of the layer. See Figure 3.2 below for a schematic of the structures of each sample type.

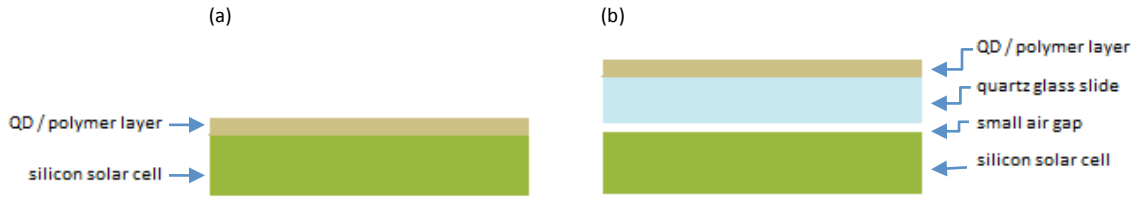

Figure 3.2. (a) Schematic of direct-coat sample. For this sample, after Kapton tape is applied to a small portion of the bus bar, the silicon solar cell is directly coated with the quantum dot and PLMA mixture. (b) Schematic of a sample with glass slide. This type of sample incorporated a thin quartz glass slide onto which the quantum dot and PLMA mixture was coated. No Kapton tape was used for this sample type. A small air gap was inevitably created in each of the samples of this type due to the irregularities in the surface topology of the silicon solar cell.

The solutions were directly spin coated onto the solar cells via the polymer spin station and hot plate. Prior to spinning, we applied Kapton tape to prevent the quantum dot solution

from completely covering the bus bars during spin-coating. This gave us direct contact points for IV measurements using the bus bars that served as the front contacts of our diced cells. We cut the tape to the approximate width of the bus bar and covered 3 to 4 mm of both ends, while making sure that some of the tape extended beyond the edge of the cell. This enabled easy removal of the tape after the layer had been applied.

After the bus bars were covered, we cleaned the cell with nitrogen gas and placed it on top of the vacuum chuck in the polymer spin station. To obtain the final desired thickness on top of the solar cell, we deposited twelve drops of the quantum dot and PLMA mixture onto the middle of the sample and started the spin station. We programmed the polymer spin station to spin at 500 RPM for 10 seconds and 6000 RPM for 60 seconds. For both spin speeds, we use a constant acceleration speed of 10 RPM/millisecond until we achieved the final spin speed.

After spinning, the samples were taken from the vacuum chuck and the direct-coated samples were heated with a hot plate at 180°C for 20 minutes to cure the layer and evaporate any remaining toluene. After 20 minutes, the samples were taken from the hot plate and laid to cool for another 5 minutes. Then, the Kapton tape was removed carefully with tweezers. Control cells also underwent the same steps of spinning and heating, but without any layer deposition.

The samples with glass slides were prepared similarly. The glass slides were wiped with acetone and then dried with nitrogen gas. The wettability of the glass slides for the QD/PLMA solution was significantly stronger than that of the solar cells, so only half the previous amount of solution was used to cover the slides. Because of the ridges and bus bars in the solar cell, the additional contact angles inhibited the solar cells from being a strong wetting layer[37]. The solutions on top of the glass slides solidified in real time, so the glass slide samples were left to dry for 5 minutes without heating, and we considered them ready for measurement after this step.

3.4 Modeling Downshifting

We developed a series of MATLAB scripts to simulate the effects of a luminescent quantum dot layer on top of a solar cell. We calculated the expected performance of a QD layer to examine the effect of fluorescence using the following properties of the system: the solar spectrum, cell EQE measurement, index of refraction of the cell, bandgap of the quantum dots, and parameterized values for the absorption/emission efficiency of the quantum dots. We varied the bandgap and absorption/emission efficiencies of the QD layers to find the properties that optimized their fluorescence and to simulate the cell generating the maximum current. Thus, we could determine the required QD bandgap and layer thickness/QD concentration of the QD-PLMA film. We also compare commercially available QD data sheets to our results and simulate the application of these QDs to our cells. Further, we compared the modified EQE of solar cells with a QD layer to the measured EQE of the cells tested in the laboratory.

3.4.1 Calculation Approach

We simulated the sun's spectrum using the AM 1.5G solar spectrum provided by NREL[12]. Depending on its wavelength, a photon from the sun may or may not hit the solar cell as a result of atmospheric scattering. Figure 3.3 shows a simplified flowchart for a photon, whose energy is greater than the bandgap energy of the semiconductor making up the solar cell. A photon received from the sun first hits the cell's QD layer. If the layer does not absorb the photon, it passes through the layer unaffected, ready to be absorbed in the cell. Otherwise, the photon is absorbed within the QD layer and is either emitted at a lower energy into the solar cell or does not get emitted by the layer and never hits the cell. The photon may also be emitted by the layer away from the cell, in which case it is also lost. Hence, a photon received from the sun has three ultimate actions: it does not hit the solar cell, it hits the cell with its original energy, or

it hits the cell with a lowered energy. However, we note that all the photons discussed here are above the bandgap energy of the semiconductor and thus generate electron-hole pairs upon absorption within the solar cell regardless of their energy.

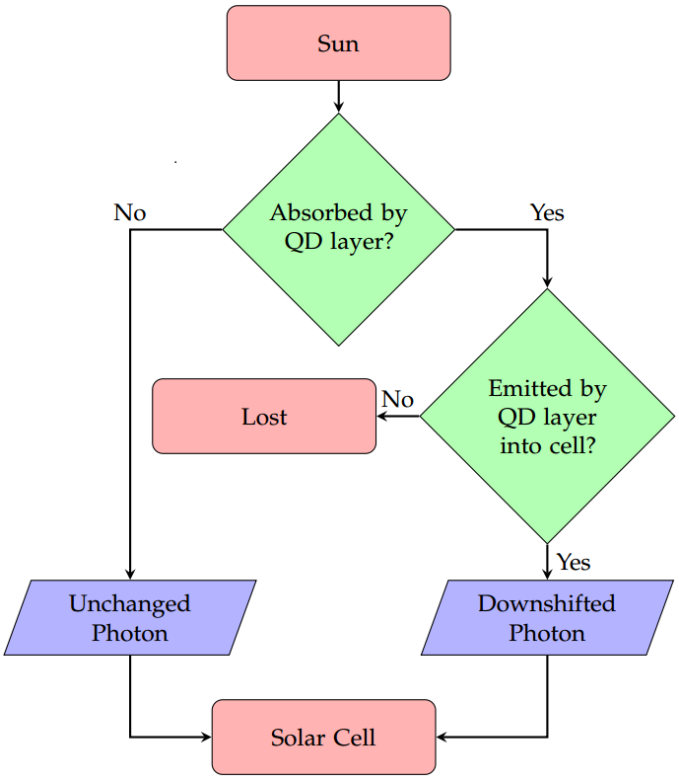

Figure 3.3. A flowchart of how a photon progresses toward the solar cell. A photon performs one of three possible ultimate actions: it does not hit the solar cell, it hits the cell with its original energy, or it hits the cell with a lowered energy. The ultimate action depends on two factors. The first factor is whether the photon gets absorbed by the QD layer. The second factor is whether the photon, if already absorbed, gets emitted by the QD layer.

A photon from the sun first reaches the cell's QD layer. If the layer absorbs the photon, it is either emitted as a photon with the bandgap energy of the QD or it does not get emitted. Otherwise, the photon passes through the layer unaffected and impinges on the cell. The probabilities the photon has of being absorbed by the QD layer and of being emitted by the QD depend on its wavelength and how we model the layer. Here we define the absorption function, $A(\lambda)$, as the probability that the QD layer absorbs a photon of wavelength λ. We also define the

emission function, $E(\lambda)$, as the probability that a photon of wavelength λ is emitted by the QD layer.

We take different approaches to modeling the quantum dots. In each modeling approach, the important aspects are the absorption and emission of the quantum dot layer, which vary with wavelength.

The first QD absorption model is a simple step function given by:

$$A(\lambda) = \begin{cases} AE, & \lambda < \lambda_{BG} \\ 0, & \lambda \geq \lambda_{BG} \end{cases}, \quad (1)$$

where AE is a constant value representing the absorption efficiency of the QD layer, and λ_{BG} is the wavelength of the bandgap of the modeled QDs.

For our calculations we set AE = 0.8 (i.e. 80% of the incident photons in the wavelength range are absorbed by the downshifting layer) and use three different QD bandgaps: 1.9 eV, 2.1 eV, and 2.3 eV. Though this simplified absorption curve shape (Figure 3.4) differs significantly from that of actual quantum dots, it is useful for seeing general trends and as a best case scenario (when emission efficiency is 100%) for comparison purposes. In addition, this approach is easy to modify: absorption efficiencies and emission wavelengths/efficiencies can be easily adjusted and explored.

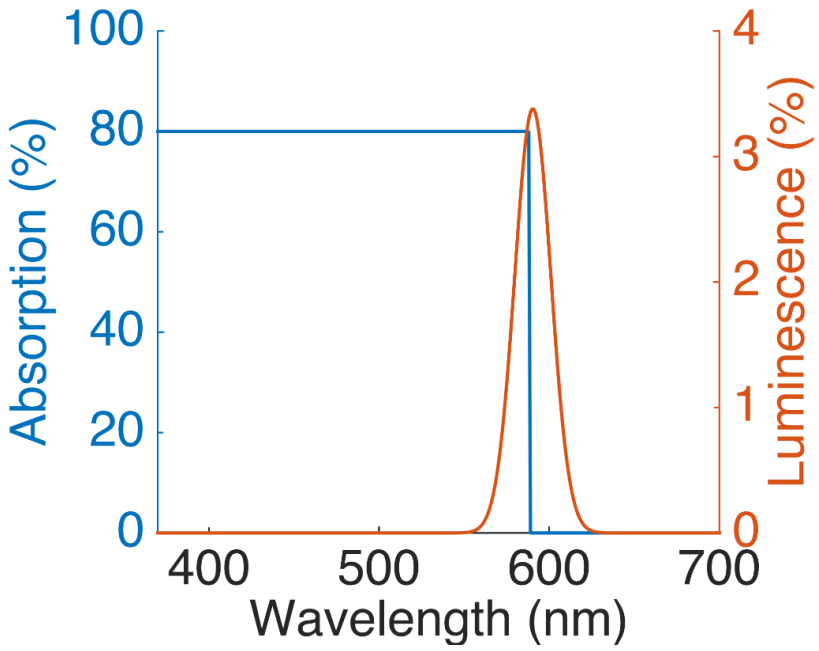

Figure 3.4. Simple downshifter model with step function absorption and Gaussian emission.

The second quantum dot model (Figure 3.5) is based on experimental data provided by an industrial supplier (CdSe/ZnS core-shell quantum dots from Ocean Nanotech) [36]. This data is used to compare to the first case in order to analyze the accuracy of the results. One caveat is that the curve depends on the amount of quantum dots being used. A thicker layer of quantum dots will absorb more photons than a thin layer. Thus, the vertical scaling of an efficiency plot is dependent on the film thickness. By choosing an appropriate vertical scale, the experimental quantum dot data can be used in our calculations.

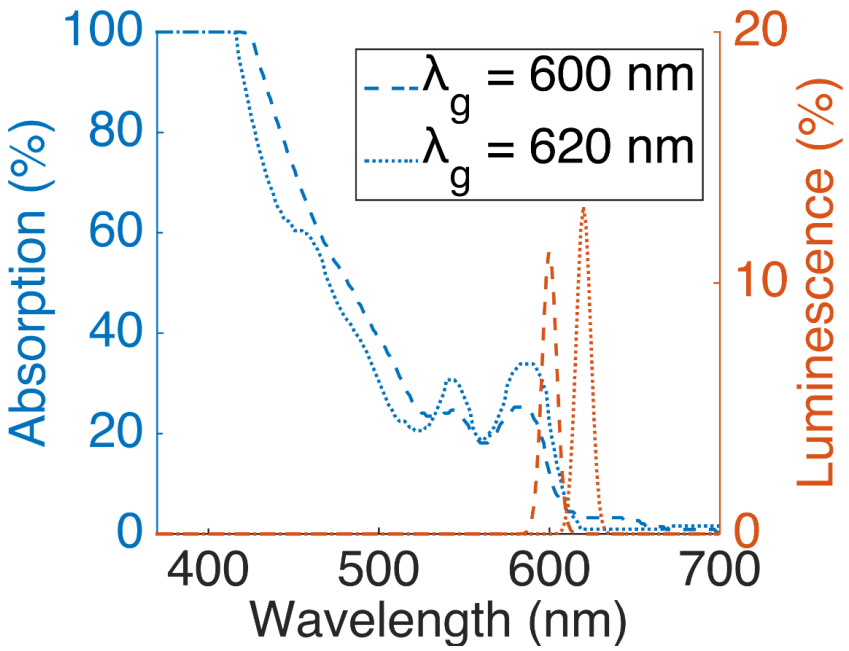

Figure 3.5. Experimental data with absorption and emission curves.

The third model of the quantum dot layer simulates the absorption using the Drude-Lorentz model. To find the formula for the absorption curve, we first calculate the electrical permittivity of the material, which describes the material's optical response to an applied electric field. Because incoming light is an oscillating electromagnetic field, the permittivity of a material affects how light propagates and how it's absorbed. The Drude-Lorentz model has the permittivity of a material relying on various oscillator modes, and it is given by:

$$\epsilon(\omega) = \epsilon_\infty - \frac{{\omega_p}^2}{\omega(\omega+i\gamma)} + \sum_{i=1}^{3} \frac{\epsilon_i {\omega_i}^2}{{\omega_i}^2 - 2i\omega\delta_i - \omega^2}\ , \qquad (2)$$

where ϵ_∞ is the permittivity at infinite frequency, ω_p is plasma frequency of the material, ω is the angular frequency of the incoming light, γ and δ_i are damping factors, ϵ_i is the strength of the i-th oscillator, and ω_i is the i-th resonance frequency.

In our calculations, we set $\epsilon_\infty = 1$, and $\omega_p = 0$ because there are no free carriers inside this material, $\epsilon_1 = 0.033$ F/m, $\epsilon_2 = 0.034$ F/m, $\epsilon_3 = 1.11$ F/m, $\delta_1 = 1.02\times10^{14}$ rad/s,

$\delta_2 = 2\times10^{14}$ rad/s, and $\delta_3 = 1.18\times10^{15}$ rad/s. We then calculate the complex refractive index n of a material, which is given by $n = \sqrt{\epsilon}$. The extinction coefficient κ is the imaginary part of the refractive index, i.e. $\kappa = Im(n)$. The absorption in this QD layer can be written using the Beer-Lambert law of absorption:

$$A(\omega) = e^{-\frac{2\omega\kappa(\omega)Md}{c}}, \tag{3}$$

where c is the speed of light, M is the molar concentration, and d is the distance that the photon travels (the thickness of the layer). For our calculations, we substituted the product $M \cdot d$ for an arbitrary absorption efficiency variable.

While the basic absorption profile is obtained from experimental data, the bandgap and Drude-Lorentz function can be adjusted to match the expected behavior of different bandgap QDs. This model provides more realistic quantum dot behavior than that of the simple scenario, while still having the ability to change the bandgap and absorption efficiencies for later calculations.

While the absorption curves differ drastically between each of the three scenarios, the three emission curves all follow a Gaussian distribution centered at the quantum dot's bandgap. Emission is defined here as the fraction of photons emitted to photons absorbed. The emission spectrum is given by:

$$E(\lambda) = EE\ \frac{1}{\sigma\sqrt{2\pi}}\ e^{-\frac{(\lambda-\lambda_{BG})^2}{2\sigma^2}}, \tag{4}$$

where EE is a constant value representing the emission efficiency of the QD layer. An EE value of 0.7 would mean that the downshifting layer emits 70% of absorbed photons. The standard deviation σ is related to the full width half maximum of the distribution of emission from our downshifting layer.

3.5 Experimental Data Collection

3.5.1 IV Testing / Solar Simulator

One method we used to determine the efficiency of our solar cells is a current-voltage measurement. A current-voltage measurement, better known as an IV measurement, is a standard technique used in the solar industry as part of a number of tests that can characterize the way a photovoltaic cell operates. Specifically, an IV measurement allows one to determine the maximum output power and hence the efficiency for a device. By conducting the experiments described in this section, we obtain data necessary to make conclusions about the performance of our solar cells and the effect that the fluorescing layer will have.

3.5.2 Experimental Structure

We performed several tests on our samples, including controls, for each experimental batch. The objectives of the experiments were different for each batch, and ranged from the addition of a pure polymer layer, to the addition of a pure QD layer, to the variation of concentrations of QD in the polymer layer, to variation of layer thickness, etc.

The experiments were structured around three phases: preliminary data acquisition and testing, systematic variation of parameters, and final data acquisition to enable observation of changes. For a typical experiment, a baseline was established by obtaining a reliable IV-curve for each sample. After applying the layer under study or varying the chosen independent variable, we conducted a second set of IV measurements and compared the results with the results obtained by the control samples.

3.5.3 Experimental Set-up

We used a Newport Model 91159 Full Spectrum Solar Simulator with an AM1.5G filter to illuminate our cells. A Keithley 2440 Source Meter was used to vary the voltage and obtain IV

curves. LabVIEW-based Oriel IV-test software from Newport enabled seamless integration between test equipment and a computer workstation for data collection.

An IV curve is a plot showing the measurement of the current (I) the cell generates as a function of voltage (V). The cell behaves similarly to a diode. The current, voltage, and power are dependent on the characteristics of the rest of the circuit the cell is in, particularly the resistive load. We adjusted the solar simulator and an AM1.5G filter to illuminate our test cells with an intensity of approximately 1 sun. The exact intensity varied between testing sessions, but we measured it with a NREL (National Renewable Energy Laboratory) calibrated silicon reference cell and recorded the result.

Before measuring any cells, we allowed the solar simulator lamp to warm up for approximately thirty minutes, to ensure greater stability in light intensity during testing. An IV measurement was obtained for the reference cell before each set of trials. This allowed for any artifacts to be detected within the system and provided us with a way to quantify the intensity of the simulator lamp, in units of suns. This value was entered into the software parameters for the test cells before measuring each new cell so that accurate efficiency calculations could be made. Between the setup of the solar simulator and the software driver, it was determined that each test would run for approximately 6.0 seconds, collecting a sweep of 60 data points. Using a variable resistive load, the solar cell was subjected to voltages ranging from -0.1 V to 0.65 V. For each cell measurement, we ran the solar simulator to collect data from three consecutive trials, waiting five minutes between trials to allow the cell to return to its original temperature before proceeding. This allowed us to ensure consistency in data and to include realistic error bars on our graphs. Pure indium metal was used to create a good electrical connection between the busbar of the solar cell and the simulator probe attachment. To prevent degradation over time

due to the oxidation or contamination of the indium, a new sliver was cut for each day of testing, or when appropriate.

For every individual test, the solar cell was placed directly in line with the aperture of the solar simulator light source. The location and orientation of the sample was standardized between tests. The sample was placed on a copper vacuum chuck, which served as a stable mounting apparatus as well as the electrical connection for the back cell contact. We based our experiment on the four-point measurement technique, but modified it for logistical reasons.

The typical four-point measurement technique uses two separate probes for current and voltage on the front contact of a photovoltaic cell. For the rear contact, the conductive block or base is used for current measurement, but a separate probe is used for voltage measurement. Refer to Figure 3.6 for a diagram of our setup.

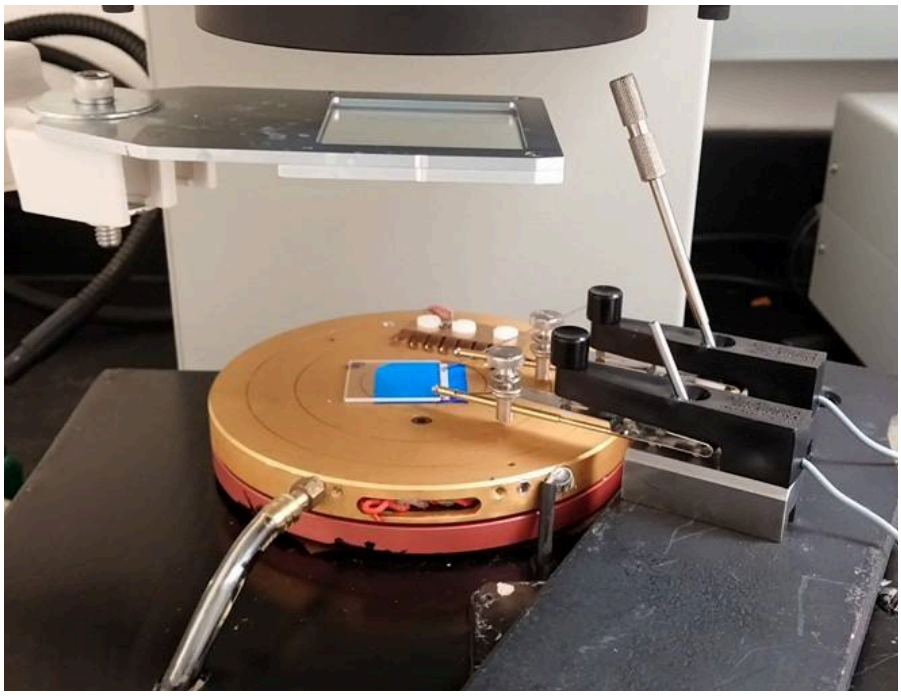

Figure 3.6. Depiction of the four-point IV Newport Full Spectrum solar simulator setup. We adjusted the solar simulator and an AM1.5G filter to illuminate our test cells with an intensity of approximately 1 sun. Two leads connect to the cell's bus bar, and another two connect to the rear current contact and the rear voltage probe.

We adapted this technique by using two points of contact on the top busbar, as specified in the four-point measurement technique, but with both the contact and voltage probes connected to the rear block. We did not observe that this modification affected our ability to collect consistent data. Through rigorous testing, it was determined that the best placement for these points of contact on the top busbar was to have the probes far apart from each other.

Thus, we placed the probes on opposite ends of the solar cell busbar, on areas that had been previously taped off using Kapton tape prior to coating with the polymer layer. This enabled us to establish a direct electrical connection between the probes and the top busbar of the solar cell with a minimum of contact resistance. For samples with a glass layer, we positioned the glass slide so that electrical connection could still be established with the probe tips while minimizing the impact on measurement accuracy.

We used the Keithley 2440 Source Meter to sweep through a range of resistive loads while the cell was under illumination. By measuring the resulting currents and voltages, we could plot an IV curve (Figure 3.7) for the cell. These results could be used to calculate the short circuit current, open circuit voltage, power output, and efficiency of the cell. We could then measure the improvement in PV cell performance by comparing the change in variables such as short circuit current and efficiency after applying our layer.

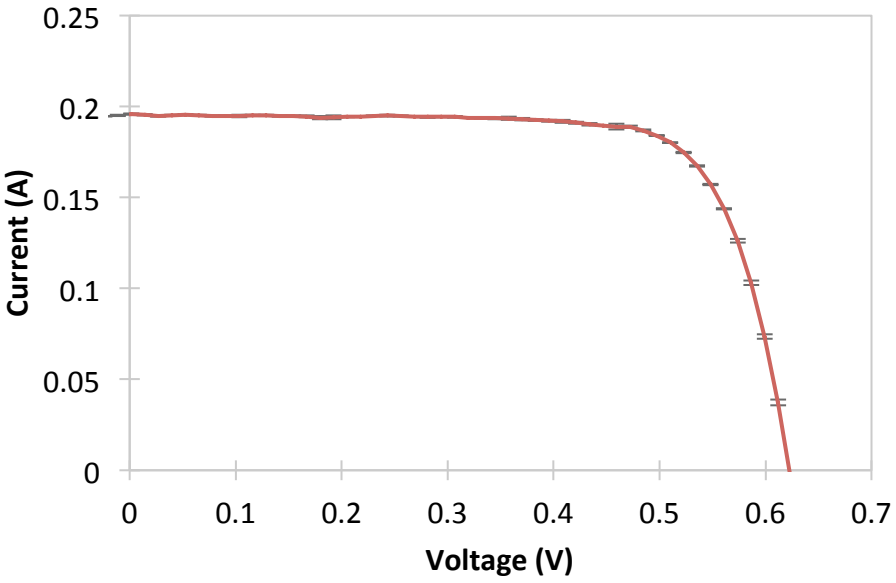

Figure 3.7. A sample IV curve from one of our cells. This cell showed a short circuit current of approximately 0.194 A with a fill factor of 75.8% and 14.0% efficiency. This curve is the result of an average of 3 tests with error bars shown as horizontal lines.

3.5.4 EQE Testing

Another method we used to determine the efficiency of our solar cells is an External Quantum Efficiency (EQE) measurement. An EQE measurement is another standard technique used in the solar industry that can further characterize the way a photovoltaic cell operates. More specifically, an EQE measurement allows one to calculate the ratio between the number of charge carriers collected by the cell and the number of photons that hit the cell. This ratio is then used to determine the efficiency of the cell at each wavelength.

3.5.5 Experimental Structure

Similarly to IV measurements, we performed several tests on our samples, including controls, for each experimental batch. The objectives of the experiments were different for each batch, and ranged from the addition of a pure polymer layer, to the addition of a pure QD layer, to the variation of concentrations of QD in the polymer layer, etc.

The experiments were also structured around three phases: preliminary data acquisition and testing, systematic variation of parameters, and final data acquisition to enable observation of changes. For a typical experiment, a baseline was established by obtaining preliminary EQE readings at differing wavelengths. After applying the layer under study or varying the chosen independent variable, we conducted a second set of EQE measurements and compared the results with the results obtained by the control samples.

3.5.6 Experimental Set-up

The set-up we used to conduct the EQE measurements was located in the Munday Lab in the Institute for Research in Electronics and Applied Physics at the University of Maryland. Major components of this system include a monochromator, lock-in amplifier, optical chopper, beam splitter, lamp, detectors and relays, sets of lenses, and other electrical connectors, as shown below in Figure 3.8.

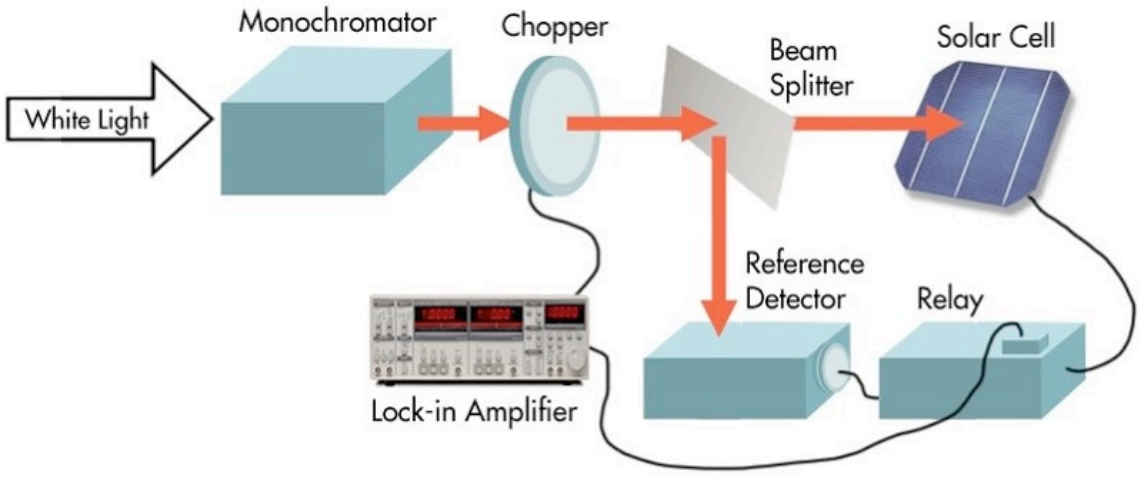

Figure 3.8. Schematic of EQE measurement set-up.

To begin EQE measurement, first we turned on the apparatus and the corresponding power sources. We used a program made in LabVIEW for collection of the EQE data. Then we checked the standard settings on the lock-in amplifier, such as the time constant. A sample cell

for measurement was attached onto the testing plate using tweezers and copper tape. We also let approximately 0.5 mm of the cell hang off the edge of the testing plate, leaving the bottom contact of the cell accessible for measuring resistance of the system. Using the LabVIEW program, we calibrated the laser beam to have a wavelength of 500nm, and focused the light onto the center of cell, close to the front contact. Afterwards, we connected the cell to the computer, and measured the resistance of the front and back contacts using the multimeter to ensure no electrical shortages in the system, as shown below in Figure 3.9.

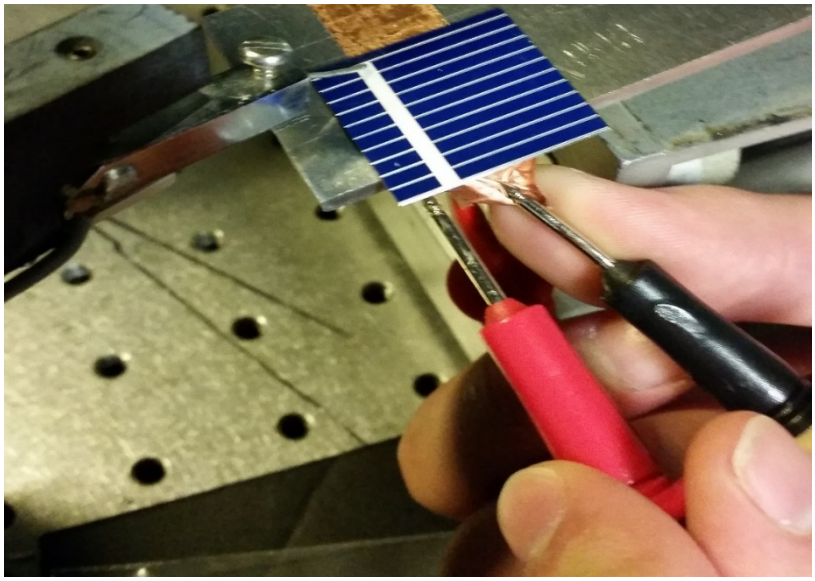

Figure 3.9. Picture of a sample cell during resistance measurement.

Additionally, it is necessary to ensure that no metal component of the system touches the measured cell, which could potentially result in faulty data due to a short circuit. After finishing the set-up process, we used a black cardboard box to isolate the cell from exposure to external light. The LabVIEW software was used to automatically control the system to measure the EQE of the cell over a desired range of wavelengths of light. Upon completion, the box was removed, and the cell was removed from the plate using a razor blade, taking care to not fracture the cell.

3.6 Potential Threats to Validity of Results

Although we believe our results are consistent and valid, we discuss potential threats to the accuracy of our findings and our efforts to mitigate these risks below.

Though we chose to use a randomized control group pretest-posttest design, we could not divide cells in a truly random fashion due to practical reasons – we assigned cells to groups in the order that we diced them from the larger 5" x 5" cells. This assignment method poses a potential threat to our internal validity. However, the pre-test values for all of our cells are similar. Hence, we concluded that our assignment method did not noticeably decrease our internal validity.

Another potential threat to internal validity is QD degradation in PLMA. In one case, we tested a cell that had been coated with a QD/PLMA layer two months prior to testing. Thus, we could not determine how much of a change in cell performance was due to our treatment and how much was due to environmental factors such as QD degradation that had occurred in the intervening two months. The effect of degradation of the QD/PLMA layer is an interesting avenue for future work.

A third potential point of concern is variation in measurements due to machine inconsistencies. It is expected that IV measurements will vary from test to test, because it is extremely difficult to recreate the exact parameters and conditions over many tests. To minimize machine variation in the IV setup, we devised a procedure by which we were able to calibrate the machine to the same operation state for each test, thus ensuring consistent and accurate results. This included fixing the relative positions of the cell and AM1.5G filter under the lamp, as well as allowing the lamp to stabilize for twenty minutes after start-up before beginning testing.

Additionally, EQE measurements were also expected to vary from test to test due to

small inevitable changes in the setup; the shifting of lenses or the degradation of the light source over time could impact the data. In order to minimize machine variation in the EQE setup, a new reference detector measurement was taken before each day of testing which would account for any changes in the light path. All other parameters such as the laser beam placement were kept as constant as possible.

As with all research projects, ours was limited by time, money, and available resources. Therefore, we chose one particular aspect to test and ignored the other potentially important aspects. Hence, a few factors threaten our population external validity: (1) using a particular set of Si cells only, (2) using only particular wavelength QDs, and (3) using a particular size of QDs. We hope that future researchers will study the impact of these factors.

Our ecological external validity is understandably poor—we cannot predict how our layer will perform in front of environmental factors such as rain or temperature variation during the day. Because the scope of our project did not extend outside the laboratory, we cannot accurately assess our ecological external validity.

3.7 Summary of Methodology

We would like to see whether a QD/PLMA solution applied to a cell that already has an anti-reflection coating will increase the cell's power conversion efficiency under sunlight. In addition, we would like to see at which QD concentration the solution has the greatest effect.

To measure gains in power conversion efficiency in treated cells, we measure the EQE and IV curves of each cell before and after layer treatment. Specifically, we use a randomized control group pretest-posttest design. For each cell, our procedure is roughly as follows. First, we measure the cell's EQE and IV curves. We then apply our QD/PLMA layer (unless the cell is in

the control group, or the cell is to be coated with just PLMA) onto the cell. Finally, we again measure the cell's EQE and IV curves. Once we collect these data for all of our cells, we test for significant gains in power conversion efficiency.

CHAPTER 4 – RESULTS

4.1 Photovoltaic Performance Calculations

We predicted the performance of solar cells with quantum dot layers in MATLAB to determine the best experimental quantum dot parameters. To do so, we approximated the absorption and emission spectra of QDs with different bandgap energies. Our first model considered a simple downshifter, where the QDs absorb light with energies above its bandgap and emit photons at the bandgap with a Gaussian distribution. For the second model, we fitted experimental QD spectral data to a Drude-Lorentz oscillator model and used the resulting relationship between oscillator terms to predict QD performance.

4.1.1 EQE Improvement

In this section we model the effect of a luminescent QD downshifting layer on the External Quantum Efficiency (EQE) of a cell. In Figure 4.1a, the experimental EQE of an unmodified Si cell is shown with the modeled EQEs of systems with a simple downshifter overlaid, each with 80% absorption efficiency (AE) and 90% emission efficiency (EE). We see that by inserting a downshifter between the light source and the cell, efficiency improves in the short-wavelength region. The small decrease in efficiency near the downshifter's bandgap happens because the downshifter "steals" photons that would have otherwise been absorbed efficiently by the cell.

In Figure 4.1b, the EQE of an unmodified Si cell is shown with the EQEs of systems modified with an overlaid Drude-Lorentz downshifter of 90% emission efficiency. Similar to Figure 4.1a, we see that by adding a downshifter in between the light source and the cell, efficiency improves in the short-wavelength region. Again, there is a small decrease in efficiency near the downshifter's bandgap (in the "middle" wavelengths).

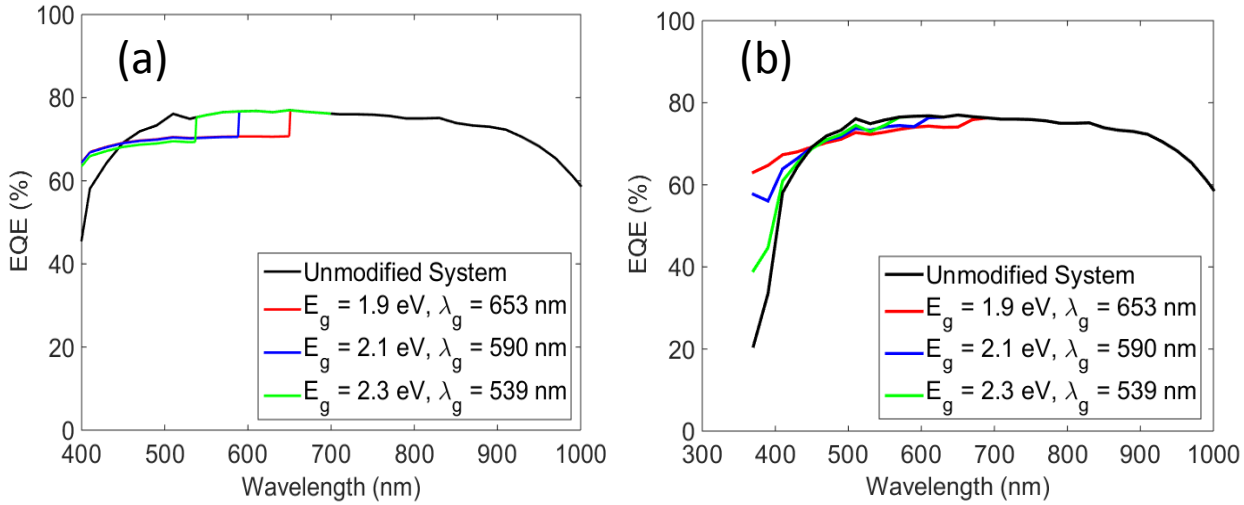

Figure 4.1. Side-by-side comparison of EQE of an unmodified Si cell and three modified Si cells under the simple downshifter model (a) and under the Drude-Lorentz model (b) Each downshifter has 90% emission efficiency.

4.1.2 Current Generation

In Figure 4.2a the contour plot shows the improvement (or regression) of current generation in several Si cells modified with a simple downshifter, over their baseline currents. This is for an absorption efficiency of 80%. We can also see that the baseline short circuit current of the Si cell is 294.5 A/m^2. The surprising finding is that any downshifter with emission efficiency below 80%, regardless of its bandgap, will decrease the cell's current generation.

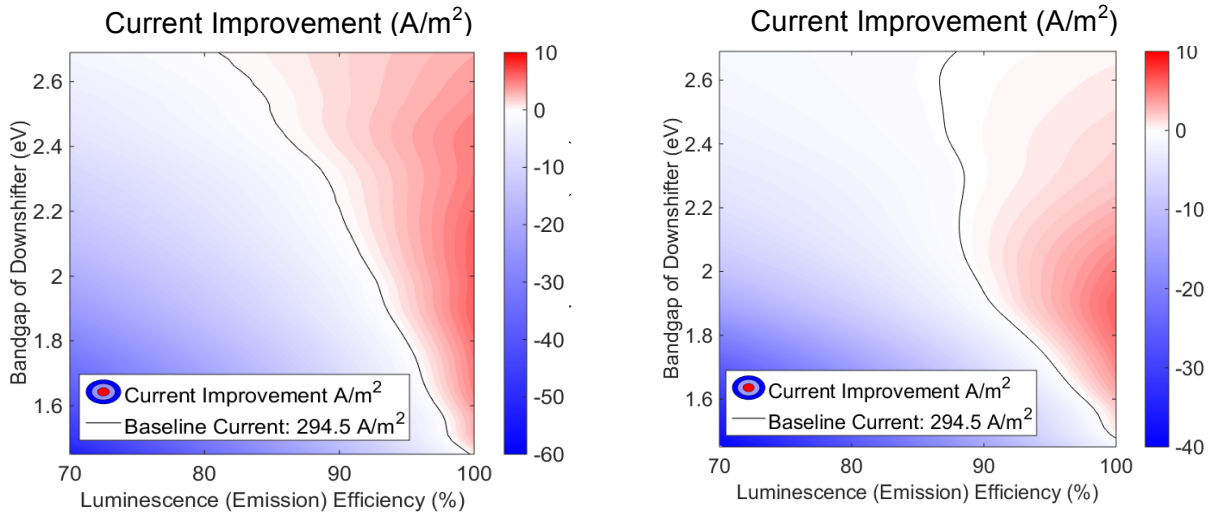

Figure 4.2: Contour plot of current improvement in Si cell with simple downshifter (a) and Drude-Lorentz downshifter (b).

Figure 4.2b shows the effect of a Drude-Lorentz downshifter. We obtain similar results: for a Drude-Lorentz downshifter with emission efficiency below 90% and for a simple downshifter with an emission efficiency below 85%, regardless of its bandgap, will decrease the cell's current generation below its baseline of 294.5 A/m^2.

We present a graphical summary of the impact of absorption and emission efficiencies on current generation in a simple downshifter in Figure 4.3. As before, for any given absorption and emission efficiency pair, the bandgap with the highest corresponding current generation is found through a brute-force search through possible bandgap values. Thus, the contour plot shows the optimal current generated by a commercial Si cell overlaid with a simple downshifting layer of a certain quality. We see that a perfectly efficient downshifter (AE = EE = 100%) will increase current by about 15 A/m^2, but even absorption and emission efficiencies around 70% will only increase current by a few amperes per square meter. There is only significant improvement for very high quality downshifters.

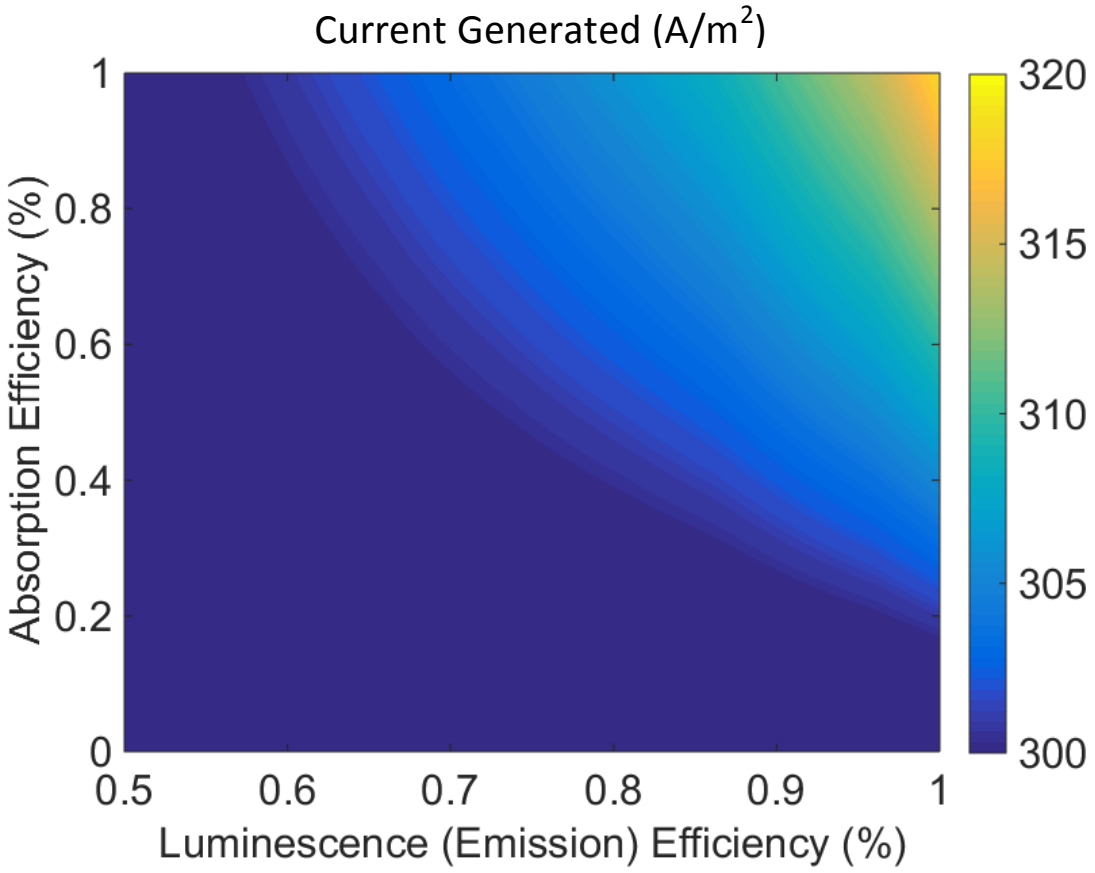

Figure 4.3. Contour of current (A/m^2) as a function of absorption and emission efficiency of layer. Maximum improvement in current for given AE and EE, with optimized bandgap energy, for the Si cells used in our experiments.

Furthermore, we performed similar calculations for perfectly efficient downshifters coated onto various other cells. We examined their effects on a generic commercial GaAs cell, as well as high efficiency cells from PV cell efficiency tables published by Green. Specifically, we considered a monocrystalline Si cell from SunPower and a polymer cell from Toshiba [38,39]. The results are displayed as the amount of current improvement that would result from using simple and Drude-Lorentz bandgap-optimized downshifters. We also performed the same calculations using absorption and emission spectra data from technical data provided by Ocean Nanotech on their CdSe/ZnS Core/Shell QD product (Figure 4.4). While there is some improvement, it is relatively low considering these results are for perfectly efficient QDs.

4.1.3 Final Calculation Results

From these results, we determined that we should coat the cell with a highly-efficient quantum dot layer; the layer should have an absorption efficiency over 60% and an emission efficiency over 90%. With a perfect layer, our calculations indicated that we could expect to see a 8.1% increase in current; however, using more realistic parameters, our model predicted a roughly 6.7% increase in current.

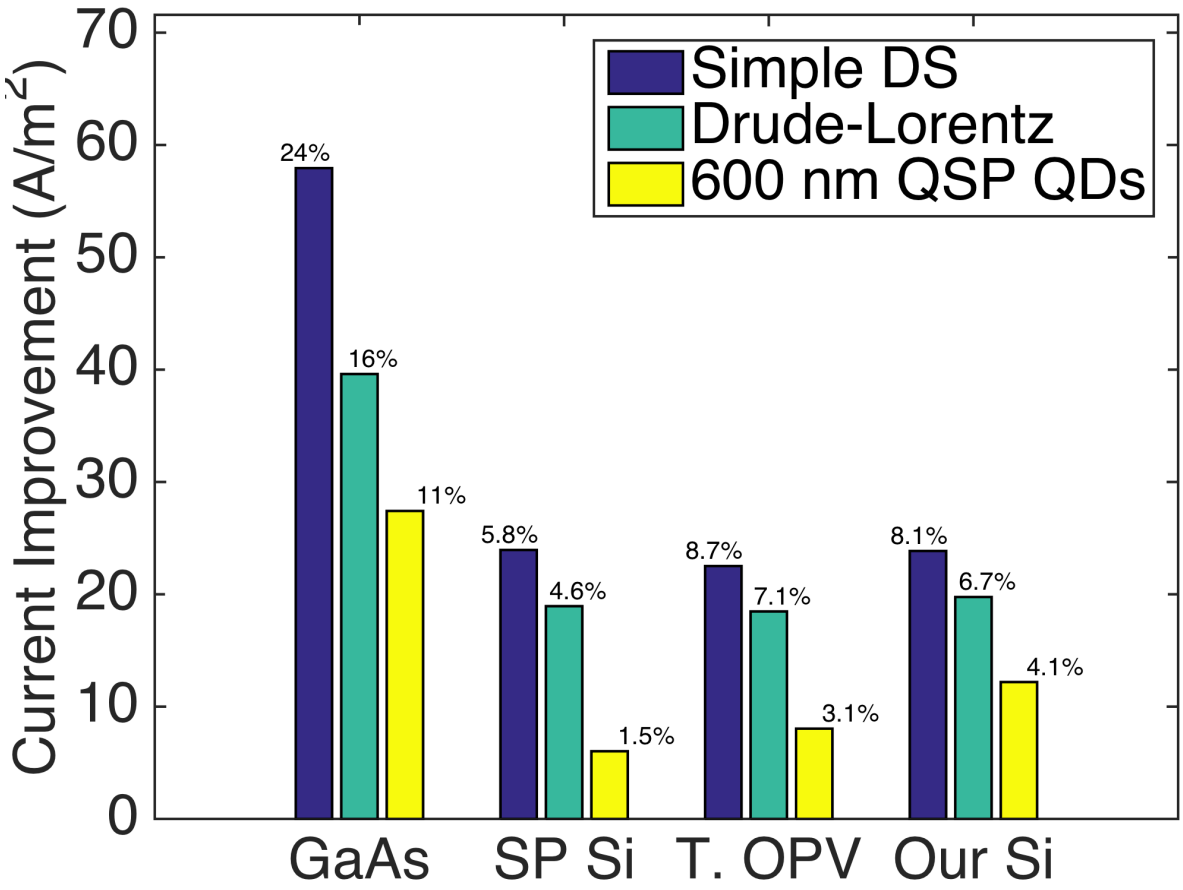

Figure 4.4: Maximum current improvement in perfectly efficient (AE = EE = 100%) downshifters. Results for bandgap-optimized simple and Drude-Lorentz downshifters are shown alongside sample data from CdSe/ZnS Core/Shell QD from Ocean Nanotech with a bandgap wavelength of 600 nm. Current improvement is relatively low, especially for high-performance cells.

4.2 IV Measurements

4.2.1 Experimental Parameters

After determining the ideal quantum dot parameters, we tested our calculations by coating solar cells with a PLMA and quantum dot solution. We tested cells ranging in efficiency from 12% to 14%. To measure the current and voltage of our experimental cells, we generated IV plots using a solar simulator to illuminate our cells. Several important parameters can be extracted from a current-voltage measurement, including the power conversion efficiency (η), short circuit current (I_{sc}), open circuit voltage (V_{oc}), and fill factor (FF).

Our focus was on the short circuit current. We examined this value instead of power conversion efficiency because measurements of power conversion efficiency are sensitive to the quality of the electrical contact between the cell and the measuring instruments. In contrast, short circuit current measurements are robust to the amount of resistance in the circuit, and changes in short circuit current are directly proportional to changes in power conversion efficiency for the same cell. This is because we can assume that the open circuit voltage and fill factor are inherent characteristics of the solar cell; any layer we add to the cell should only change the power by changing the short circuit current.

To define things clearly, the short circuit current, I_{sc}, represents the current generated when there is no voltage drop over the load, seen as the current axis intercept on the IV curve (i.e. the current when the circuit is shorted). The short circuit current is useful because it is proportional to the number of charge carriers generated per unit time, which should be the characteristic directly increased by a properly implemented luminescing layer. The short circuit current was easily obtained from the IV data and gave us a solid measure of comparison. The efficiency from the LabVIEW program was not used because we found that the value depended heavily upon the fill factor, which was a measure of the connection between the probes and the

bus bar. Thus, increases in efficiency of the solar cell later mentioned in this chapter refer directly to increases in the short circuit current.

Note that the IV plots contained in this subsection are based on the raw data only, without normalizing for lamp intensity. While we calibrated the lamp to illuminate the cells with an intensity of 1 sun, there were non-trivial fluctuations in intensity over time, on the order of about ±0.02 suns over the course of 3 to 4 hours. However, we did measure the lamp intensity before and after each cell measurement. Thus, we could normalize our short circuit current measurements by dividing them by the lamp intensity at the time of measurement (estimated as the average of the intensity before and after). This value would represent the short circuit current per sun of illumination.

Also, note that we only normalized our data for the trials using direct coating onto the cell. Later trials using glass slides did not include normalization because the measurements could be taken in much shorter timeframes in which the fluctuation in lamp intensity was negligible. Thus, the short circuit measurements were comparable without needing to normalize for lamp intensity.

The layers we applied to the solar cell to increase the efficiency and current generated consisted of CdSe/ZnS quantum dots suspended in a poly-lauryl methacrylate (PLMA) solution. The QD/PLMA solution dried after being applied to the top face of the solar cell, forming a solid fluorescent film. The polymer provided a protective medium for the QDs to be suspended in, preventing degradation of the QDs.

4.2.2 PLMA Layer on Bare Cell

Before testing the QD/PLMA layer all together, we investigated the effect of a PLMA layer with no QDs added. By comparing the current of a cell before and after PLMA coating with a bare cell, we noted that the PLMA made no substantial change in the cell's short circuit current, as seen in Figure 4.5. By taking the standard deviation of the cell's current measured over multiple trials, we calculated error bars to determine this significance.

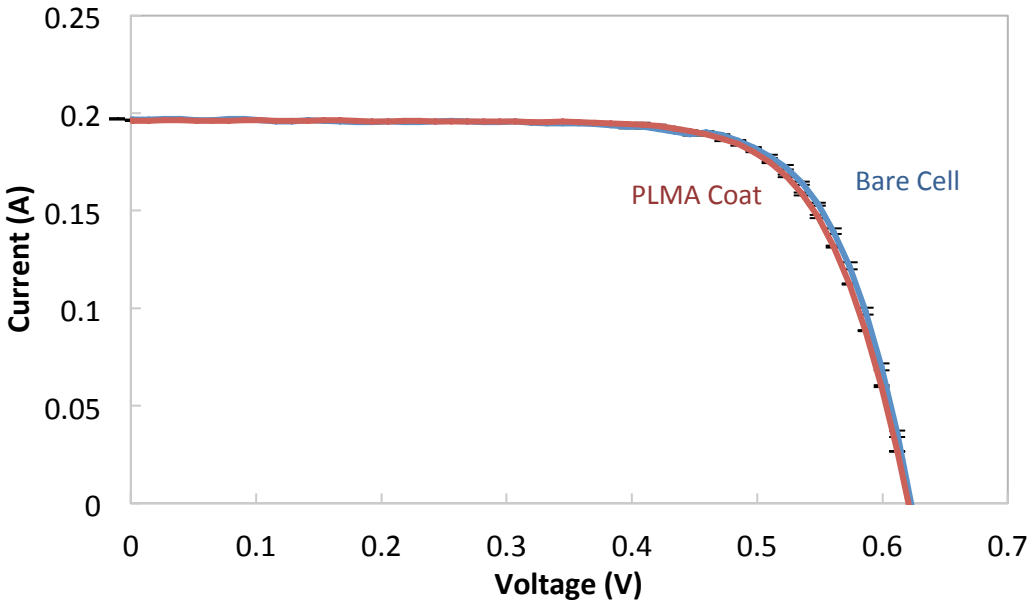

Figure 4.5. Full IV plot of a Si solar cell coated with PLMA. The PLMA insignificantly increased the cell's short circuit current from $I_{sc} = 0.196 \pm 0.002$ A/sun to $I_{sc} = 0.198 \pm 0.002$ A/sun. The A/sun units correspond to normalizing the current by the incident number of sun's illumination, which could vary by up to a few percent between measurements.

PLMA's negligible effect on short circuit current can be explained as a counterbalance of two factors. PLMA has an index of refraction between that of the cell and that of air. In general, such a gradient increases the amount of light that enters the cell. On the other hand, the PLMA layer is smoother than the commercial anti-reflection coating, which increases light reflection and hence offsets the effect of the index of refraction gradient.

4.2.3 Cell with QD/PLMA Layer Coated Directly

After establishing a basis for the negligible effect of the PLMA layer alone, quantum dots were added to the PLMA solution with the same deposition conditions in the previous section. Because of the florescent properties of QDs, we expected the solar cell efficiency to increase. Ideally, short wavelength photons, which have little chance of turning into current, would be absorbed by the QD layer and re-emitted at longer wavelengths. These longer wavelength photons are more likely to generate electron-hole pairs, increasing the overall current generated. However, this improvement depends on several quantities including film thickness, QD efficiency, and QD concentration. The following scenarios show the impact of these parameters.

4.2.3.1 Low Efficiency QDs & Low Concentration

The first quantum dot layer we tested consisted of 45% quantum yield QDs with a concentration of 1 mg/mL QD/PLMA. As with the pure PLMA layer, this 1mg/mL QD/PLMA layer did not change in short circuit current of the cell (Figure 4.6).

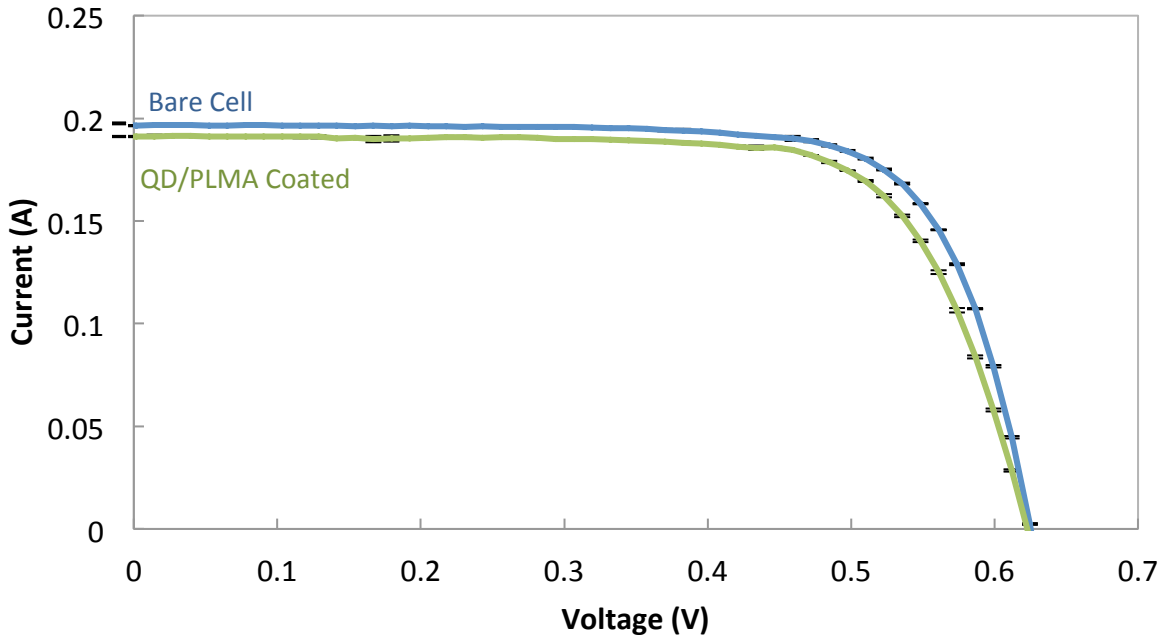

Figure 4.6. Full IV plot (not adjusted for lamp intensity, which was measured and varied by at most a few percent between runs) of a Si solar cell coated with 1 mg/mL QD/PLMA mixture using low quality QDs. After adjusting for lamp intensity, this layer did not change the cell's short circuit current (I_{sc} = 0.191 ± 0.003 A/sun became I_{sc} = 0.191 ± 0.003 A/sun).

4.2.3.2 Low Efficiency QDs & Higher Concentration

Using a layer with a low concentration of low efficiency QDs, we saw no change in the cell's current. We decided to increase the concentration of quantum dots in the layer in order to increase the influence of the quantum dots. Instead of the 1 mg/mL QD/PLMA used before, we applied a layer with twelve drops of 5 mg/mL QD/PLMA concentration (Figure 4.7).

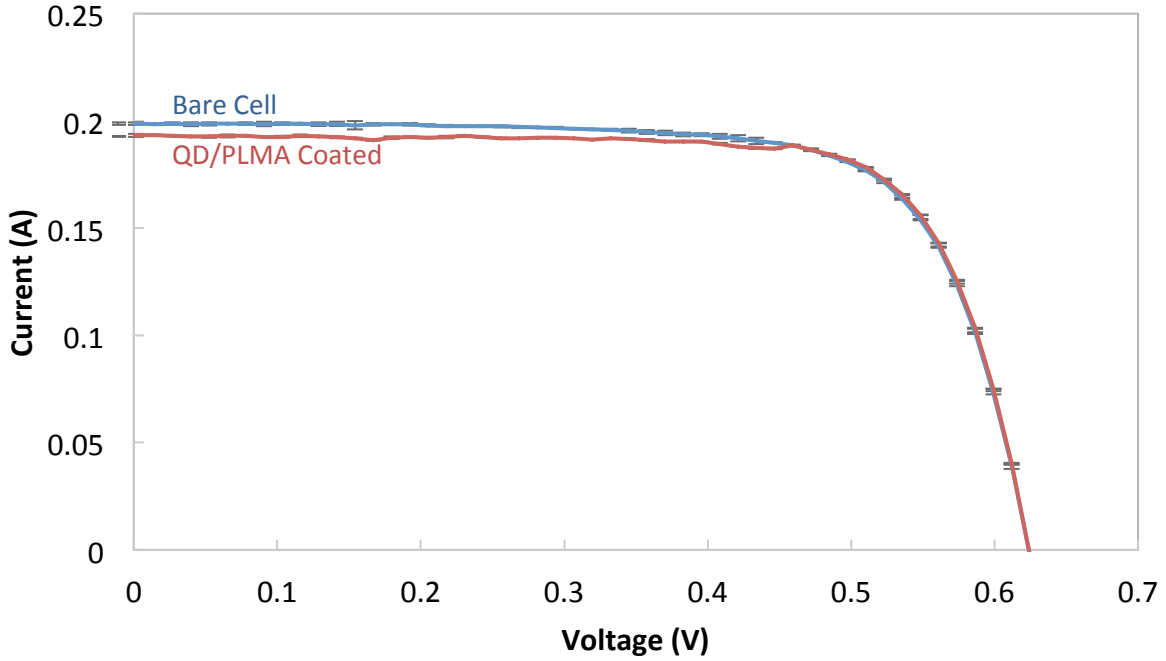

Figure 4.7. Full IV plot of a Si solar cell coated with 5 mg/mL QD/PLMA mixture using low quality QDs. After adjusting for lamp intensity, this layer decreased the cell's short circuit current from $I_{sc} = 0.191 \pm 0.002$ A/sun to $I_{sc} = 0.186 \pm 0.002$ A/sun.

We saw that current began to decrease with more QDs. An explanation for this new current decrease is that the QDs are of too low quality. With more low quality QDs, more short wavelength photons get absorbed and not emitted by the QDs. With fewer low quality QDs, more of these short wavelength photons avoid getting absorbed by the QDs and have a chance of turning into current. Other quantum dot research showed promise with 5 mg/mL, however, so we sought to determine whether our layer thickness or our QD concentration was at fault.

4.2.3.3 Low Efficiency QDs & Thicker Layer

To test this idea further, we increased the QD/PLMA layer size. In terms of QD concentration we saw the same trend: higher QD concentration resulted in higher current decreases, which supported our hypothesis pertaining to our low efficiency quantum dots. The

graphs below depict data from a layer that used 12 drops of 2.5 mg/mL QD/PLMA solution, and was spun at 3000 RPM, using 520 nm QDs (Figure 4.8).

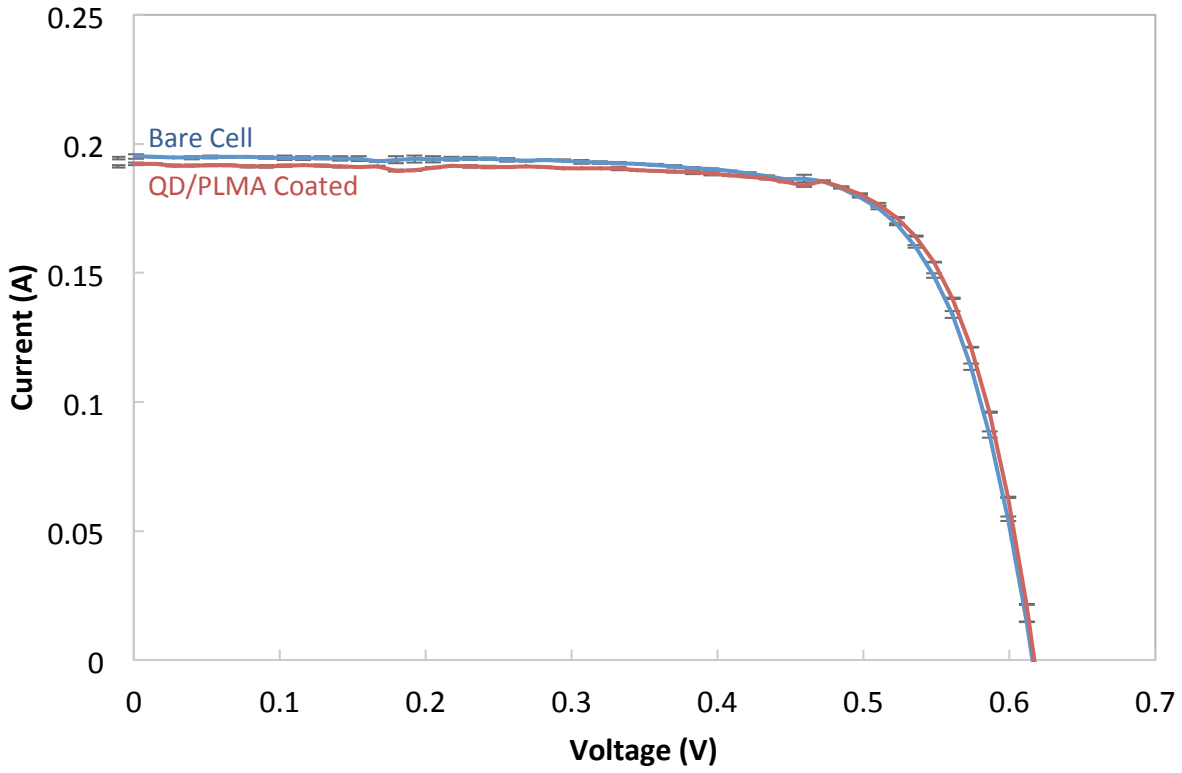

Figure 4.8. Full IV plot (not adjusted for lamp intensity, which was measured and varied by at most a few percent between runs) of a Si solar cell coated with 2.5 mg QD/mL PLMA layer. After normalizing for lamp intensity, the thicker QD/PLMA layer decreased the cell's short circuit current from $I_{sc} = 0.1919 \pm 0.0014$ A/sun to $I_{sc} = 0.1880 \pm 0.0022$ A/sun.

We also explored the effect of the overall layer itself. Regardless of parameter changes, the layer itself may have been harming the cell's inherent anti-reflection layer, and thereby decreasing the current.

To research this further, we looked at the layer through a scanning electron microscope (SEM) to note the differences in the cell texture before and after coating (Figure 4.9a). In these SEM micrographs, it can be noted that our layer fills in the anti-reflection etchings of the layer. In Figure 4.9b, the anti-reflection layer of the cell is clearly defined in the left while the layer

covers these protrusions on the right. These etchings were originally designed to reduce the reflection of the photovoltaic cell, so filling these in caused the cell to become more reflective than before and reduced the current generated.

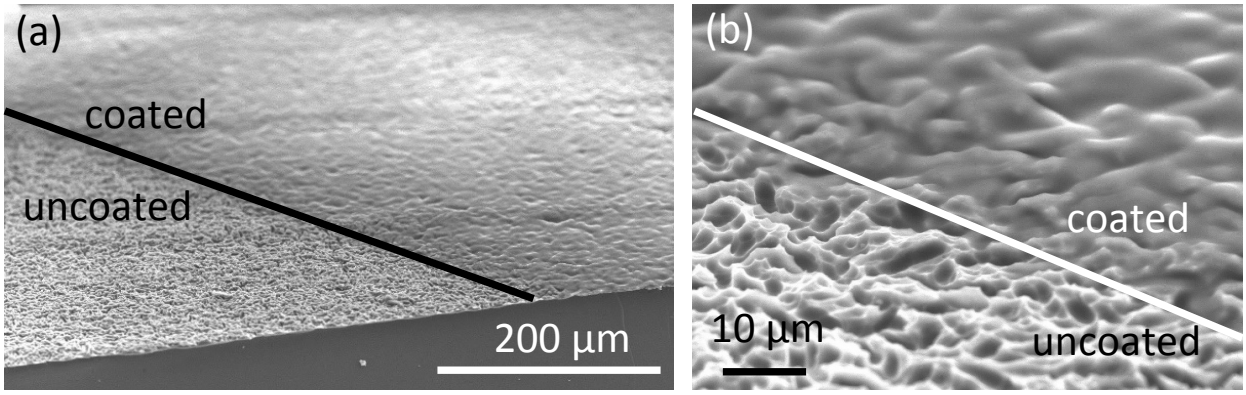

Figure 4.9. (a) SEM image of a half-coated cell. The uncoated left side is much more granular than the coated right side of the cell. (b) SEM zoomed image of a cell half coated with PLMA. The right side (PLMA) smoothes the antireflection coating, unlike the more granular left side (bare).

We therefore decided to alter our methodology by introducing a piece of glass that would be coated by our layer and then placed on top of the solar cell. In this way, we could compare the short circuit currents of a solar cell with bare and coated glass slides while controlling for the change in anti-reflection. In addition, this reduced variation within our data because only one cell would be on the IV setup at all times, as only the glass slides on top needed to be switched for each measurement.

4.2.4 PLMA Layer on Glass Slide, on Cell

We began by looking at the impact of PLMA on the glass by itself to compare this control with the QDs and PLMA on the glass together. When the PLMA was coated on the glass, it had no effect on the short circuit current generated (Figure 4.10).

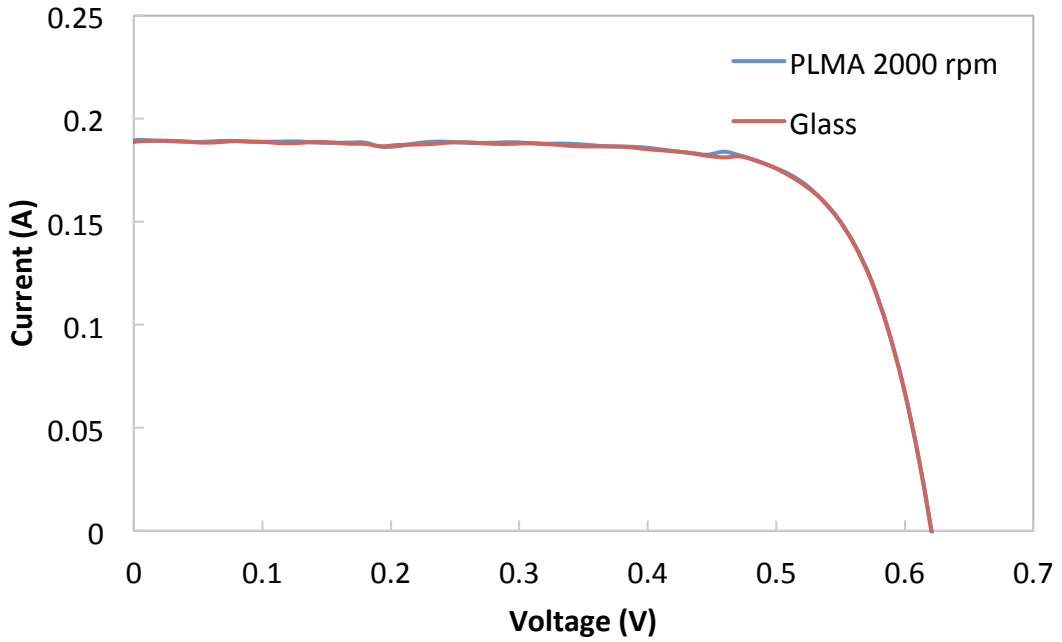

Figure 4.10. Full IV plot of a Si solar cell with bare glass slide and solar cell with PLMA coated glass slide. The PLMA was spun at 2000 RPM. The thicker QD/PLMA layer did not change the cell's short circuit current (I_{sc} = 0.1881 ± 0.0004 A/sun became I_{sc} = 0.1883 ± 0.0006 A/sun).

4.2.5 Cell with QD/PLMA Layer Coated on Glass Slide

The final step was to apply the QD and PLMA solution onto the glass and test a solar cell with the glass on top. We used high quantum yield QDs with manufacturer-reported efficiencies of over 85%, which were much higher quality than the QDs used previously. Using these high efficiency quantum dots at a high concentration with different spin speeds, we attempted to create layers similar to the layer required by our theoretical calculations. Because solution concentration and spin speed are interchangeable parameters that affect efficiency, we chose to control the spin speed while maintaining the concentration at 20 mg/mL QD/PLMA. We planned to vary spin speeds accordingly to account for the high concentration. Two different types of CdSe/ZnS quantum dots (with emission wavelengths of 520 nm and 620 nm) were spin coated onto glass slides. The same number of drops were placed in the center of each slide and the spin

speeds were varied from 750-2000 RPM. The IV curve data from these glass slides were compared to an uncoated slide as a control.

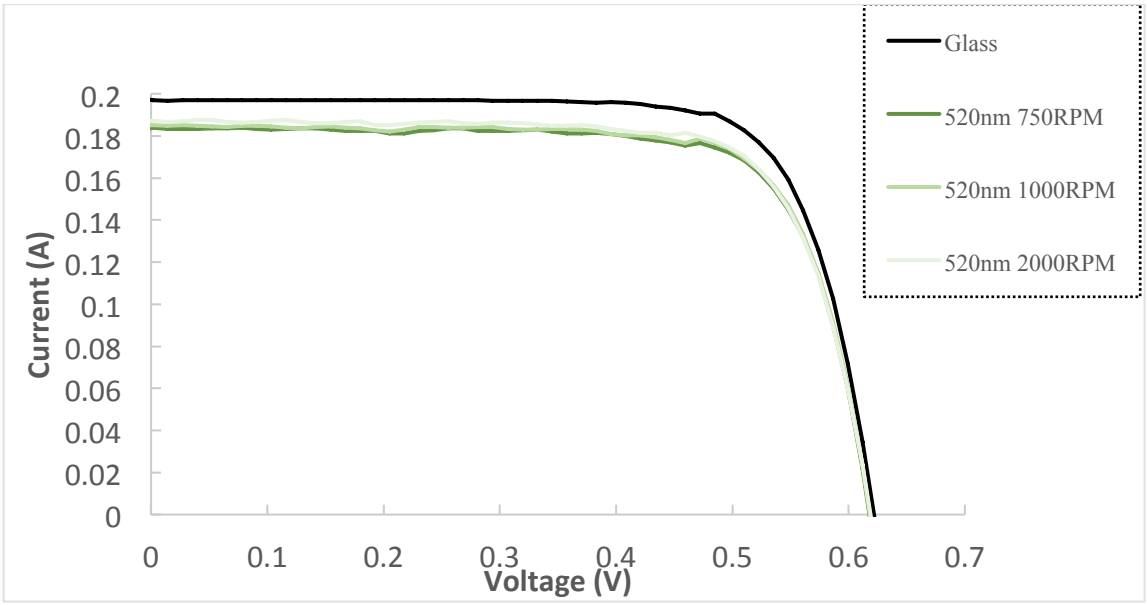

Figure 4.11. Full IV plot of a Si solar cell coated with 20 mg QD/mL PLMA layers of varying thicknesses and a QD emission peak of 520nm. The thicker QD/PLMA layers appear to decrease the cell's current generation more, but all layers decrease cell performance overall.

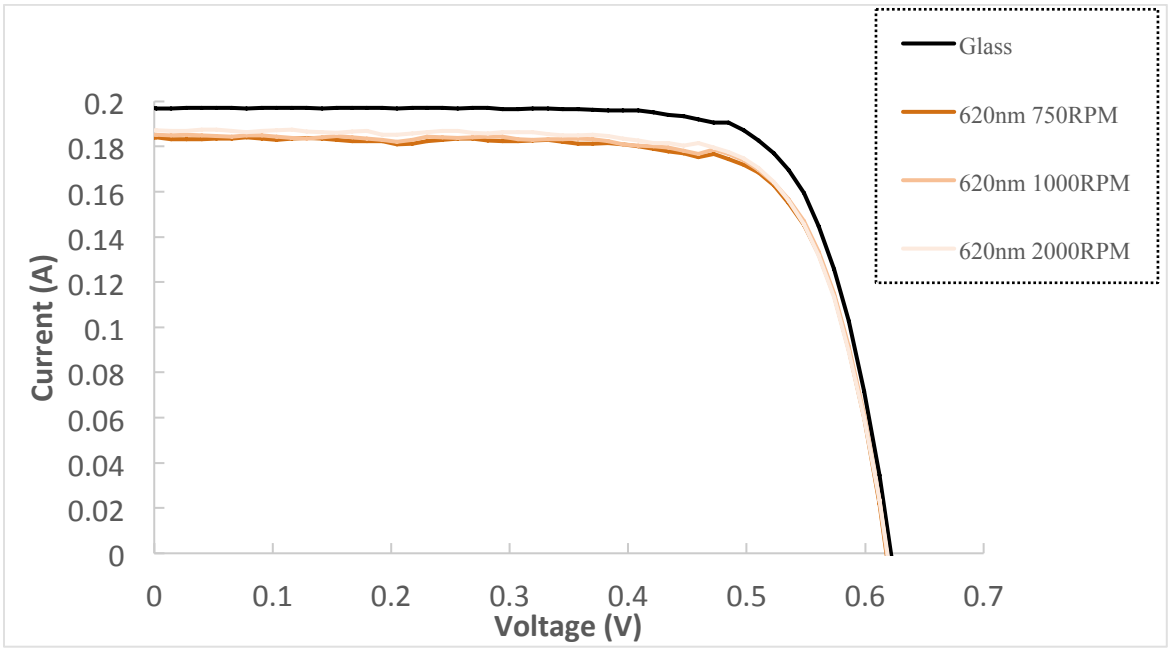

Figure 4.12. IV measurements of a Si cell coated with 20 mg QD/mL PLMA layers of varying thicknesses and a QD emission peak of 620nm. The thicker QD/PLMA layers appear to decrease the cell's current generation more, but all layers decrease cell performance overall.

With both the 520nm and 620nm QD layers, we found a drop in short circuit current across all spin speeds. We also found that our layers with the lowest spin speed (the thickest layers) produced the greatest drop in efficiency, in accordance with our model. This progressive drop can be seen in Table 4.13b. The reason the thicker layers resulted in lower current generation may have been due to the lower efficiencies of the layer. For instance, in Figure 4.12, the thinner cell spun at 2000 RPM performs marginally better than the thicker layers spun at only 750 RPM and 1000 RPM.

4.2.6 IV Conclusions

We changed various key parameters of the QD layer to explore the current generated within the solar cells. Because we did not observe increases in current with low efficiency QDs at various concentrations and thicknesses (Table 4.13a), we increased the quality of the QDs and altered the setup. However, using higher efficiency QDs also decreased current (Table 4.13b). We believe that the layer itself needs to be even more optically efficient and properly direct light into the cell. Due to the air gap between the glass slide and the solar cell, it is possible that the light was scattered to different directions. This would explain the dramatic losses in current generation, despite the improvements that we expected to see based on our theoretical performance calculations.

Table 4.1. Summary of short circuit current measurements of a Si cell coated with various layers. Note that the units are A/sun after normalizing for lamp intensity.

	Control Current (A/sun)	**Layer Current (A/sun)**	**Result**
PLMA Layer on Bare Cell	0.1957 ± 0.0020	0.1982 ± 0.0021	**No Change**
Low Efficiency QDs & Low Concentration	0.1906 ± 0.0028	0.1905 ± 0.0029	**No Change**
Low Efficiency QDs & Higher Concentration	0.1911 ± 0.0022	0.1856 ± 0.0022	**"Large" Decrease**
Low Efficiency QDs & Thicker Layer	0.1919 ± 0.0014	0.1880 ± 0.0022	**"Small" Decrease**
PLMA Layer on Glass Slide, on Cell	0.1881 ± 0.0004	0.1883 ± 0.0006	**No Change**

Table 4.2. Summary of short circuit current measurements of a Si cell coated with either 520nm QD/PLMA layer or 620nm QD/PLMA layer at various spin speeds.

	Glass/Control Current (A)	**750 RPM Current (A)**	**1000 RPM Current (A)**	**2000 RPM Current (A)**
520nm QD/PLMA Layer Coated on Glass Slide	0.1977	0.1826	0.1846	0.1865
620nm QD/PLMA Layer Coated on Glass Slide	0.1977	0.1839	0.1847	0.1875

4.3 EQE Measurements

4.3.1 EQE Measurements of Cells

We used External Quantum Efficiency (EQE) measurements to examine the effects of the QD/PLMA layer on specific wavelengths of light, as opposed to total current generated. As mentioned in previous sections, EQE shows the efficiency of converting an incident photon into a collected carrier for each incident wavelength of light. If the quantum dot layer was working as desired, the EQE would be increased for wavelengths where the quantum dots were absorbing and re-emitting into the cell. If there were no photon losses in this process and the reflection of the cell was unchanged, we would see increases in the cell's total current generation from the IV

measurements. However, the decrease in current seen in the IV measurements as a result of the added QD/PLMA layer is also found in the EQE plots of the same glass slides. The following plots show the overall decrease in EQE as a result of the layers. For the measurements below we chose to limit the range of wavelengths to 350-450 nm. We chose this range because the change in solar cell efficiency at these short wavelengths is most indicative of the QD layer's effect. It should also be noted that we completed one full EQE sweep of the cell with and without the layer. During this test we concluded that there is a negligible effect as a result of the QD layer for wavelengths longer than the emission wavelength of the QDs.

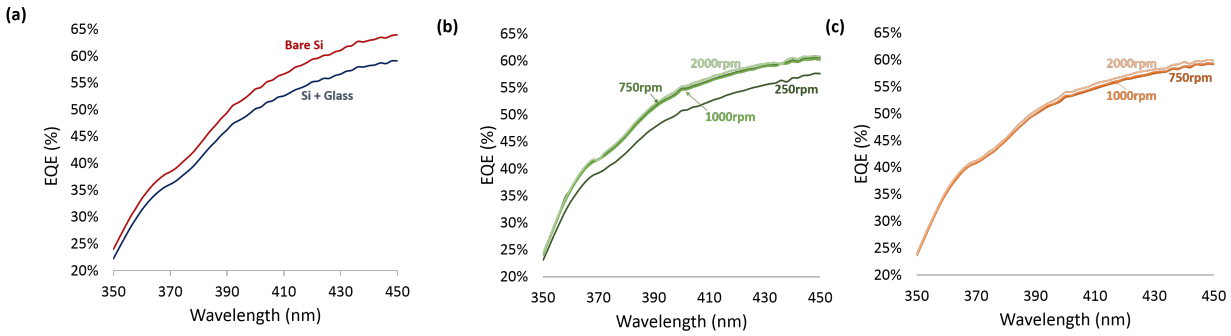

Figure 4.14. EQE comparisons of (a) Silicon cell with and without glass, (b) 520nm QD coated glass, and (c) 620nm QD coated glass.

This set of graphs depicts the cell's efficiency with different QD coated slides. Figure 4.14a depicts the EQE of a bare silicon cell and the same silicon cell with a glass slide on top. The glass slide covered cell served as our control to isolate the effect of the quantum dots. Figure 4.14b shows the EQE of the same cell with the 520 nm emission wavelength QD layers spun at different speeds. For high quality QDs that efficiently emit into the solar cell, this region of the spectrum should have increased EQE. Unfortunately, this is not the case, presumably due to low luminescence efficiency of the quantum dots or poor optical coupling of the emitted photons to the solar cell. This data shows that four drops of solution spun at the fastest speed of 2000 RPM

performed the best out of the four layers at short wavelengths (i.e. it had the smallest decrease in EQE). Meanwhile, the layer coated at 250 RPM performed the poorest. Figure 4.14c corroborates the conclusions drawn from Figure 4.14b because the same trend is exhibited with the 620 nm emission wavelength QD layers. However, because 2000 RPM was the highest tested spin speed (and all rates led to a decrease in the EQE), we cannot conclude that our data set includes the optimum spin speed.

4.3.2 EQE of QD Coated Slides Compared to Control

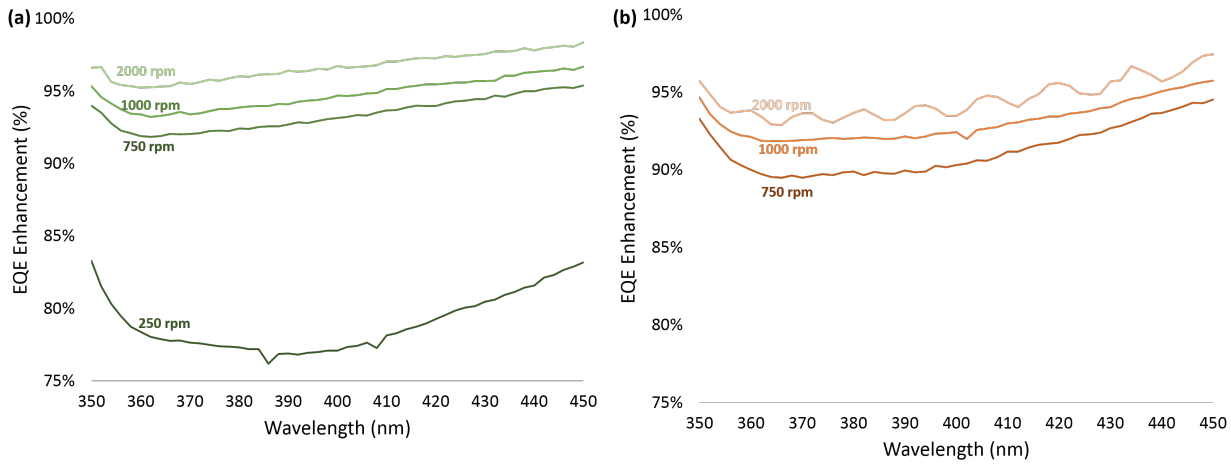

Figure 4.15. Ratio of (a) 520 nm emission wavelength QD coated slides to control and (b) 620 nm emission wavelength QD coated slides to control.

Figure 4.15 shows the EQE enhancement resulting from the addition of QDs to a glass slide on top of the Si solar cell. In Figure 4.15a and Figure 4.15b, the cell exhibits a decrease in efficiency for all wavelengths from 350-450 nm. It appears that the 2000 RPM spin speed had the smallest decrease in efficiency for the shorter wavelengths, yet still resulted in a net decrease in efficiency. The drip coated slide of 620nm coated QDs exhibited the most significant decrease in efficiency, which we determined to be due to the coating containing significantly more QDs than any other sample. Because none of these slides exhibited an increase in the efficiency of the solar cell at the short wavelengths, we cannot conclude that our QD/PLMA layer had a positive impact on the performance of the cell.

4.3.3 EQE of QD Coated Slides Compared to Control with Index Matching Fluid

The effect of the air gap between the bottom of the glass slide and the top of the cell has a significant negative effect on the number of photons that enter the cell. Due to concerns about the reflection between the top of the cell and bottom of the glass slide, we also placed an index matching fluid between the cell and glass slide, as shown in Figure 4.16 below.

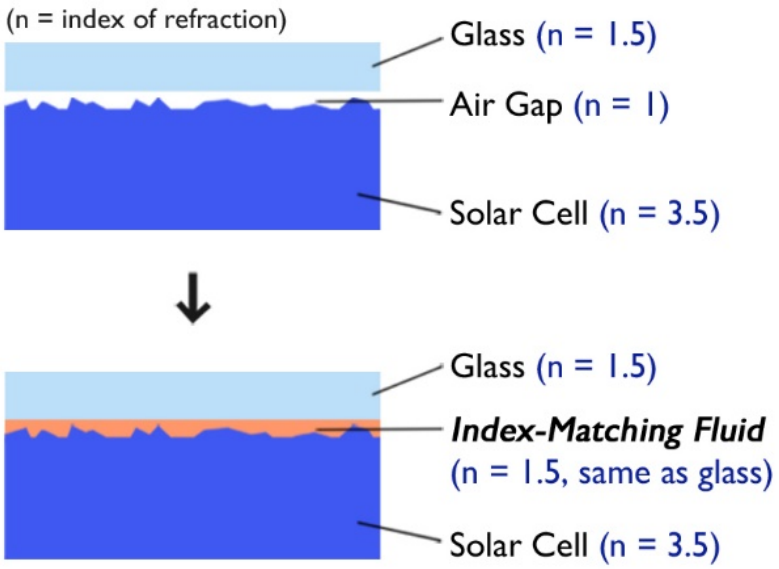

Figure. 4.16. Air Gap between Glass Slide and Cell with Index Matching Fluid

In absence of this index matching fluid, an air gap introduced a drop in the index of refraction between the cell and glass slide, which increased reflection at the interface of the materials. Hence by increasing the index of refraction between the glass slide and the cell, this index matching fluid reduces reflection of the light emitted by the QDs when compared to the cell with glass slide without the fluid.

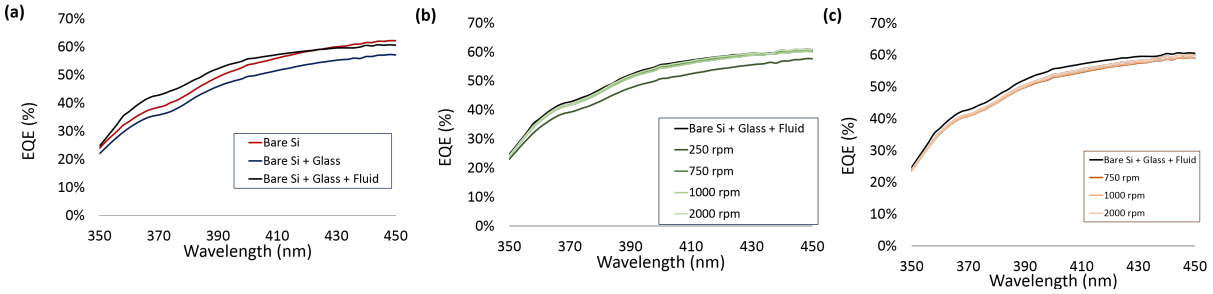

Figure 4.17. Index matching fluid EQE measurements for (a) the control, (b) 520 nm emission wavelength QDs, and (c) 620 nm emission wavelength QDs.

As seen in Figure 4.17a, the index matching fluid increased the efficiency of the control to the point where it actually increased the efficiency of the cell with the glass slide above even the bare silicon solar cell at wavelengths shorter than 420 nm. At wavelengths greater than 420 nm, however, the efficiency dropped below that of the bare cell. In both Figure 4.17b and Figure 4.17c, the QD layer coated cell exhibited lower efficiencies than the control; however, the 520 nm quantum dots were very close to the same efficiency as the control. This effect can be seen further in Figure 4.18.

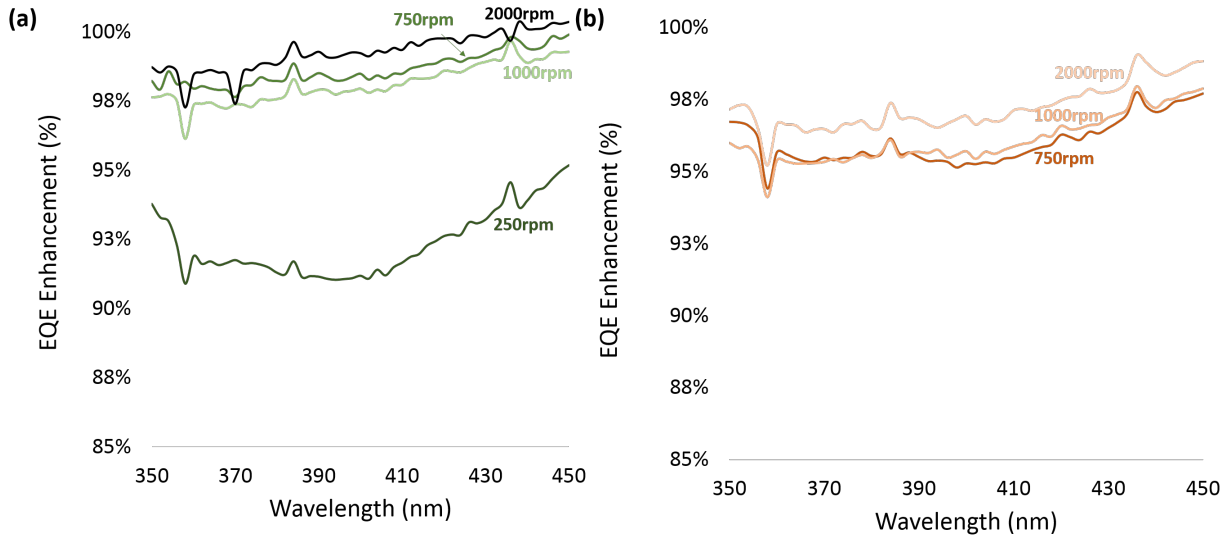

Figure 4.18. Ratio of (a) 520nm QD (b) 620nm QD coated slides to control with index matched fluid.

Figures 4.18a and 4.18b display the ratio of the efficiency of the layers compared to the efficiency of the control. This data shows that even with the addition of an index matching fluid between the glass slides and the top of the cell, the QD layer still decreased the efficiency of the cell. There could be a number of reasons why no efficiency increase was seen due to applying a QD layer. These reasons will be discussed in the section below.

4.4 Discussion of Results

We refer back to Fig. 4.2b and note that even with a high absorption efficiency of 80%, QDs should reduce the current generated by a cell if the emission efficiency is below 80-90%. Moreover, these results apply to QDs with optimized bandgaps - realistically the regression of current will be even greater. Our experimental results support these observations. We see from our EQE enhancement data (Fig. 4.15, 4.18) that the QD layer decreased efficiency for short wavelengths. Combined with the full wavelength sweep, we can conclude our QDs failed to increase the efficiency for any wavelength. We note that because the overall absorption and emission efficiencies of the layer are less than called for by the theoretical calculations, we expect to see a decrease in current generation. The IV results show that the short-circuit current for these cells was also significantly reduced. Testing with varied layer thickness and QD concentration provides similar results. The common property of the tested layers is their low quantum yield, that is, excess photons are absorbed by the layer and not reemitted into the cell.

Based on our analysis, we have determined that there are a number of factors that can improve future QD layers. The first thing that can improve the effect of the layer would be to use high emission efficiency QDs (i.e. QDs with an emission efficiency greater than 90%). This is an extremely important factor, especially for thicker layers, due to the potential for photons to be reabsorbed by the QDs. High emission efficiency QDs can somewhat combat this effect by

increasing the total number of photons emitted into the cell. This would have an overall positive effect on the layer's performance.

In addition to high emission efficiency QDs, the effect of our layers could be improved by directly applying the QDs on top of the solar cell. Because our QDs were embedded in the layer and not applied directly to the cell, the QDs most likely emitted the photons uniformly in all directions. If the QDs were deposited directly on top of the solar cell, due to the substrate's significantly higher index of refraction compared to glass or PLMA, the QD photon emission would be preferentially directed into the substrate. One other potential way to harness this effect while maintaining the benefits of the PLMA layer would be to have a layer thickness on the order of a few hundred nanometers. At scales this small, it is likely the QDs would still preferentially emit downwards. By harnessing this effect, the QD layer could be improved by reducing the overall number of photons reabsorbed by the QDs, as well as the number of emitted photons that would not otherwise be absorbed by the cell.

Lastly, it is important to choose QDs that have emission wavelengths corresponding to wavelengths where the cell exhibits high EQE. This further improves the chances that the QD emitted photons will be absorbed by the cell. By carefully crafting a layer that can take advantage of these three parameters, QD layers can potentially increase the efficiency of most solar cells.

CHAPTER 5 – Conclusion

Our research sought to increase solar cell efficiency by using an external quantum dot layer as a luminescent layer to downshift the short wavelength photons to longer wavelength photons able to be better converted to current by the cell. We have simulated the physics of these devices using MATLAB scripts to perform our calculations. These calculations have provided insight into the effect of various quantum dot and layer parameters on the solar cell's efficiency and current generation. We conclude in Figure 4.2b that even quantum dot layers with 80% absorption efficiency must have emission efficiency above 80-90% for the layer to have a positive impact on the solar cell's performance, specifically for high efficiency cells with pre-existing anti-reflection coatings. For cells without a pre-existing anti-reflection coating, the required absorption and emission efficiencies of the QDs can be lower and still significantly improve the overall cell's power conversion efficiency. However, such cells are uncommon and not typically available commercially. Quantum dot manufacturers normally produce quantum dots with efficiencies greater than 50%, but they are quite rarely greater than 80%. To realize the full benefits of the quantum dot fluorescing layer for photovoltaics, these higher quality quantum dots are required.

Using computational results to drive our experiments, our team has worked extensively in the lab to explore the feasibility of using quantum dots on commercially available solar cells. The two major data collection methods we have worked with are current-voltage (IV) and External Quantum Efficiency (EQE) measurements. IV plots were useful for determining the current generated by the solar cell and its overall efficiency while EQE plots helped determine which range of wavelengths the QD layer affects. Ultimately, we were unable to demonstrate an overall efficiency increase. Using EQE measurements, we observed that the QD/PLMA layer hindered photon absorption at all wavelengths, including the short wavelengths. Ideally, with a

higher efficiency QD layer, fewer photons would be lost, and the benefit of luminescing photons at longer wavelengths would be fully realized.

After examining the performance of quantum dot layers with our theoretical calculations, we have identified the importance of using high quality quantum dots with emission efficiencies or quantum yields greater than 80%. The QDs we initially worked with had efficiencies around 45%, which we believe to be a key factor in the negative results from our earlier layers. The techniques we developed to perform our calculations have proved to be valuable for solving problems with experimental processes and remain useful for demonstrating the necessary quantum dot layer parameters for solar cell improvement. With our theoretical and experimental results, we hope to contribute to the use of QDs to enhance future solar cell designs and help make solar energy Earth's energy provider.

Sources Cited:

1. Li M. Peak Oil, the Rise of China and India, and the Global Energy Crisis. Journal of Contemporary Asia 2007;37(4):449.
2. Harries JE, Brindley HE, Sagoo PJ, Bantges RJ. Increases in greenhouse forcing inferred from the outgoing longwave radiation spectra of the Earth in 1970 and 1997. Nature 2001;410(6826):355.
3. Solomon S, Plattner GK, Knutti R, Friedlingstein P. Irreversible climate change due to carbon dioxide emissions. Proc.Natl.Acad.Sci.U.S.A.Proceedings of the National Academy of Sciences of the United States of America 2009;106(6):1704.
4. Fang X. China's Energy Crisis and the New Energy Revolution. Futurics 2005;29(3)
5. Luque A, Hegedus S. Handbook of Photovoltaic Science and Engineering (2nd Edition). John Wiley & Sons.
6. Crabtree GW, Lewis NS. Solar Energy Conversion. 2007;60:37.
7. Tsao J, Lewis N, Crabtree G. Solar FAQs. U.S. Department of Energy. 2006. Available from: http://www.sandia.gov/~jytsao/Solar%20FAQs.pdf.
8. Trupke T, Green MA, Wurfel P. Improving solar cell efficiencies by down-conversion of high-energy photons. Journal of Applied Physics 2002;92(3):1668.
9. Khan A. Device physics: A bug-beating diode. Nature 2006;441(7091):299-299.
10. Baumeister P. Optical Coating Technology. Society of Photo Optical; 2004.
11. Lin C-C, Chen H-C, Tsai YL, Han H-V, Shih H-S, Chang Y-A, Kuo H-C, Yu P. Highly efficient CdS-quantum-dot-sensitized GaAs solar cells. 2012;20(S2):A319.
12. Standard Tables for Reference Solar Spectral Irradiances: Direct Normal and Hemispherical on 37° Tilted Surface. West Conshohocken (PA): ASTM International, 2012. Designation G173-03(2012).
13. Kongkanand A, Tvrdy K, Takechi K, Kuno M, Kamat PV. Quantum Dot Solar Cells. Tuning Photoresponse through Size and Shape Control of CdSe/TiO2 Architecture. Journal of the American Chemical Society 2008;130(12):4007.
14. Tetyana T, Yuri V. Semiconductor II-VI Quantum Dots with Interface States and Their Biomedical Applications. 2011.
15. Liu Y, Xu J, Sun H, Sun S, Xu W, Xu L, Chen K. Depth-dependent anti-reflection and enhancement of luminescence from Si quantum dots-based multilayer on nano-patterned Si substrates. Optics Express 2011;19(4):3347.
16. Prasad A, Balakrishnan S, Jain SK, Jain GC. Porous Silicon Oxide Anti-Reflection Coating for Solar Cells. Journal of the Electrochemical Society 1982;129(3):596.
17. McEvoy AJ, Markvart T, Castañer L. Practical handbook of photovoltaics: Fundamentals and applications. 2012. Waltham, MA: Academic Press.
18. Iyengar VV, Nayak BK, Gupta MC. Silicon PV devices based on a single step for doping, anti-reflection and surface passivation. Solar Energy Materials and Solar Cells 2010;94(12):2205.
19. Han K-S, Lee H, Kim D, Lee H. Fabrication of anti-reflection structure on protective layer of solar cells by hot-embossing method. Solar Energy Materials and Solar Cells 2009;93(8):1214.
20. PVCDROM: First Photovoltaic Devices [Internet]. Tempe (AZ): Arizona State University Solar Power Lab: c1994-2005 [cited 2014 Jan 13]. Available from: http://pvcdrom.pveducation.org/MANUFACT/FIRST.HTM

21. Maxwell, JC. A Dynamical Theory of the Electromagnetic Field. Philosophical Transactions of the Royal Society of London 1865;155:459-512.
22. Einstein, A. Über einen die Erzeugung und Verwandlung des Lichtes betreffenden heuristischen Gesichtspunkt. Annalen der Physik 1905;17(4):132-148.
23. Millikan, RA. A Direct Determination of "h". Physical Review 1914;4(1):73.
24. 2000. Remote Sensing [Internet]. National Oceanographic and Atmospheric Administration; [cited 2014 Nov 12]. Available from: http://www.srh.noaa.gov/jetstream/remote/remote_intro.htm
25. Chartier, G. Introduction to Optics. 2005. Springer New York.
26. Chen H-C, Lin C-C, Han H-W, Tsai Y-L, Chang C-H, Wang H-W, Tsai M-A, Kuo H-C, Yu P. Enhanced efficiency for c-Si solar cell with nanopillar array via quantum dot layers. 12 Sept 2011;19(5)
27. Jung J-Y, Zhou K, Bang JH, Lee J-H. Improved Photovoltaic Performance of Si Nanowire Solar Cells Integrated with ZnSe Quantum Dots. The Journal of Physical Chemistry C 2012;116(23):12409.
28. Tang J, Kemp KW, Hoogland S, Jeong KS, Liu H, Levina L, Furukawa M, Wang X, Debnath R, Cha D and others. Colloidal-quantum-dot photovoltaics using atomic-ligand passivation. Nat Mater Nature Materials 2011;10(10):765-771.
29. Bawendi Group. 2000. Research [Internet]. Cambridge, MA: Massachusetts Institute of Technology; [cited 2015 Mar 20]. Available from: http://nanocluster.mit.edu/research.php
30. Xu WZ, Charpentier PA. Quantum Dots in Polymer Films for Light Selectivity. Volume 1034, ACS Symposium Series: American Chemical Society; 2010. p 137.
31. van Sark WGJHM. Enhancement of solar cell performance by employing planar spectral converters. Applied Physics Letters 2005;87(15):151117.
32. Richards BS. Luminescent layers for enhanced silicon solar cell performance: Down-conversion. 2006;90(9):1189–1207.
33. Raffaelle RP, Castro SL, Hepp AF, and Bailey SG. Quantum dot solar cells. Progress in Photovoltaics: Research and Applications 2002;10:433–439.
34. van Sark WGJHM, Donega, CDM, Harkisoen C, Kinderman R, van Roosmalen JAM, Schropp REI, Lysen EH. Modeling Improvement of Spectral Response of Solar Cells by Deployment of Spectral Converters Containing Semiconductor Nanocrystals. Semiconductors 2004:38(8):962-969
35. Sahu Niranjan, Parija B., Panigrahi Sreeram. Fundamental understanding and modeling of spin coating process: A review. Indian Journal of Physics. 2009 April;83(4):493-502.
36. Ocean NanoTech. QSP [Internet]. Ocean NanoTech; c2009 [cited 2015 Feb 15]. Available from: http://www.oceannanotech.com/product.php?cid=72&pid=170.
37. Hirasaki GJ. Wettability: Fundamentals and Surface Forces. SPE 1991.
38. Green MA, Emery K, Hishikawa Y, Warta W, Dunlop ED. Solar cell efficiency tables (version 42). Prog. Photovolt: Res. Appl. 2013:21:827–837.
39. Green MA, Emery K, Hishikawa Y, Warta W, Dunlop ED, 2014. Solar cell efficiency tables (version 44). Prog. Photovolt: Res. Appl. 2014:22:701–710.